Master's thesis

NTNU
Norwegian University of Science and Technology
Faculty of Natural Sciences
Department of Physics

Ingvild Svendsen

Correlation between the mean wind in the mesosphere and lower thermosphere and solar cycles

Master's thesis in Applied Physics and Mathematics
Supervisor: Patrick Joseph Espy
June 2021

NTNU
Norwegian University of
Science and Technology

Ingvild Svendsen

Correlation between the mean wind in the mesosphere and lower thermosphere and solar cycles

Master's thesis in Applied Physics and Mathematics
Supervisor: Patrick Joseph Espy
June 2021

Norwegian University of Science and Technology
Faculty of Natural Sciences
Department of Physics

NTNU
Norwegian University of
Science and Technology

Abstract

The mean wind in the middle atmosphere transports chemical species central to the energy balance in the atmosphere. Strong coupling between the layers of the atmosphere also motivates exploring the mean winds in the mesosphere and lower thermosphere (MLT) to improve climate models. By use of lagged cross-correlation and cross-spectra, the similarities in the mean wind in the MLT and the solar index $Y_{10.7}$ were explored. Hourly mean winds, at about 95 km altitude, from the radar station in Saskatoon (Canada) provided by the Super Dual Auroral Radar Network, solar intensity data, $Y_{10.7}$, from the European Space Agency and AP index from National Oceanic and Atmospheric Administration formed the raw data basis used in this report.

There was a weak, but significant correlation between the mean wind and the 27-day solar cycle in $Y_{10.7}$. However, both data sets varied with the same period, about 27-days, implying dependence of the mean wind on the variation of $Y_{10.7}$ with solar rotation. On a longer-term scale, the mean wind and $Y_{10.7}$ showed moderate correlation with $Y_{10.7}$ at a period of 13 years. The mean wind in the mesosphere and lower thermosphere is at least partly driven by solar irradiance. Furthermore, it was not possible to determine whether energetic particle precipitation was a driver of the MLT; the modelling necessary is out of scope for this thesis.

Sammendrag

Middelvinden i den midtre atmosfæren transporterer kjemiske spesier som er sentrale for energibalansen i atmosfæren. Sterk avhengighet mellom de ulike lagene i atmosfæren gir motivasjon for å utforske middelvinden i mesosfæren og den lavere delen av termosfæren for å forbedre klimamodeller. Ved bruk av tidsforskjøvet korrelasjon og kryssspekter, ble likhetene mellom middelvinden i MLT og solindeksen $Y_{10.7}$ utforsket. Timeverdier for middelvind, ved 95km høyde, fra radarstasjonen i Saskatoon (Canada) skaffet av Super Dual Auroral Radar Network, solintensitetsdata, $Y_{10.7}$, fra den europeiske romfartsorganisasjonen og AP-indeksen fra NOAA utgjorde grunnlaget for rådataen brukt i denne masteroppgaven.

Det ble funnet en svak, men signifikant korrelasjon mellom middelvinden og den 27 dager lange solsyklusen i $Y_{10.7}$. Derimot varierte begge dataseriene med den samme perioden, som indikerer at middelvinden avhenger av variasjonene av $Y_{10.7}$ som følge av solens rotasjon. Ved et lengre tidsperspektiv, viste middelvinden moderat korrelasjon med $Y_{10.7}$ ved en periode på 13 år. Middelvinden i mesosfæren og den lavere delen av termosfæren er i det minste delvis drevet av solens irradians. Videre var det ikke mulig å bestemme om energirik partikkelnedbør var en driver i mesosfæren og den lavere delen av termosfæren; modelleringen nødvendig er utenfor omfanget til denne oppgaven.

Acknowledgements

I would like to thank Patrick Joseph Espy, my supervisor, for keeping me motivated, teaching me how to write a scientific report and sharing with me some of the great amount of knowledge he has about the atmosphere, the sun and data analysis. Also, I am grateful for the patience he showed me and for being my teammate and supporter during the previous year. Finally, thanks to Patrick again and Wim van Caspel for aiding me with the source code.

Contents

List of Figures

List of Tables

Abbreviations

DFT	=	Discrete Fourier Transform
ESA	=	European Space Agency
EUV	=	Extreme ultraviolet radiation
FFT	=	Fast Fourier Transform
MLT	=	Mesosphere and lower thermosphere
NaN	=	Not a Number
NOAA	=	National Oceanic and Atmospheric Administration
SD	=	Super Dual Auroral Network
SSW	=	Sudden stratospheric warming
U	=	Zonal wind, wind in the east-west direction with positive towards east
UV	=	Ultra violet
V	=	Meridional wind, wind in the north-south direction with positive towards north

1 Introduction

The atmosphere eclipsing the earth is a coupled system. Heat, energy and chemicals in one altitude may be transferred to or affect the state of another through radiative processes, wave propagation and mass exchange [1]. Momentum deposition by gravity waves acts as a drag force and overrides the radiative forcing of the circulation in the mesosphere and lower thermosphere (MLT). The effect of solar radiation absorption and energy deposited by energetic particle precipitation in auroras also contribute to the dynamics in the MLT [2].

The primary research question to be addressed is *whether or not the solar cycles influence the mean wind in the mesosphere and lower thermosphere*. Both investigating whether the 27-day and the 11-year solar cycles are present in the meridional and zonal wind. In addition, seasonal differences in the 11-year cycle in the mean wind are examined. The final question is whether solar irradiance or energetic particle precipitation is the source of long-term variations in the mean wind.

Based on the change of sign of the temperature gradient, the atmosphere is divided into vertical layers. Starting at the surface of the earth is the troposphere, reaching up to about 10 km. Above this, the stratosphere or the ozone layer extends up to 50 km altitude. The mesosphere is located between 50 km and 85 km above the earth. Finally, the thermosphere encapsulates the earth from 85 km to 690 km height [3].

Until recent time, the convention has been to think that each layer in the atmosphere acts independently from the others. Recent studies show that the stratosphere is coupled to the troposphere, meaning happenings in the stratosphere may impact weather and climate. This is the case also for even higher regions, like the mesosphere and the thermosphere [4]–[6]. Due to the traditional mindset, the lower part of the atmosphere is a lot more investigated than the middle and upper atmosphere. To improve models for weather and climate, it is crucial to understand how the middle and upper atmosphere function and how the atmosphere as a whole is coupled. Chemical species like ozone are transported with the wind and can participate in chemical reactions in the atmosphere. Deeper understanding of the wind patterns on Earth will increase the perception of the transportation of chemical species.

During summer the stratosphere above the summer pole is heated continuously for months, due to the solar irradiance absorbed by the ozone. Differences in heating of the ozone initiate a net flow from the summer pole towards the winter pole on both hemispheres. Furthermore, the Coriolis force deflects the moving particles of air to the right on the northern hemisphere and the left on the southern hemisphere. Thus, the heating of the summer pole has the outcome of westward stratospheric flow in the summer and eastward stratospheric flow in the winter [7]. Gravity waves, see section 2.3, absorb the energy of waves with phase velocity smaller than the wind velocity

and increase exponentially in amplitude as they propagate upwards. The amplitude of the gravity wave extends into the mesosphere and eventually break and deposit momentum. The deposited momentum function as a drag force on the wind in the MLT forcing a summer to winter pole circulation in the mesosphere [2].

Inside the Sun is a magnetic field that changes direction every 11 years and does a full cycle every 22 years. Sunspots appear at mid-solar latitudes, move towards the equator and disappear during the 11-year cycle. Sunspots emit electromagnetic radiation and energetic, charged particles, measured by the solar index $Y_{10.7}$ and AP, respectively. $Y_{10.7}$ follow the eleven-year cycle, while AP has its maxima when the solar irradiance is increasing or decreasing, every six years or so. In addition to these variations, the sun is rotating with an approximately 27-day period, giving a variation of the solar irradiance with the same period.

The Super Dual Auroral Network (SD) is a series of radars at high latitudes. The radars have proven to provide reliable data for wind in the mesosphere and lower thermosphere by registering ionization trails from meteors entering the atmosphere. SuperDARN has provided data from the last 27 years, longer than any other data set. The data set in this thesis is from Saskatoon in Canada as this station proves to measure the wind accurately. It spans 1st of January 1994 to 31st of December 2016, one of few data-sets long enough to observe two eleven-year solar cycles.

The solar index $Y_{10.7}$ was derived to find variations in the energy deposited in the MLT by the solar irradiance. $Y_{10.7}$ is composed of a traditional, well-used solar index, $F_{10.7}$ which measures radio waves and two new components adding the effect of X-rays, extreme ultraviolet radiation (EUV) and Lyman-α radiation.

AP is a daily, linearly scaled index based on mid-latitude observations representing the global variations of geomagnetic activity [8]. This activity origins from energetic particle precipitation from the sun. In this project monthly values for AP are used, therefore correlation between AP and wind will only be possible to look at on a long-term scale.

Lagged correlation between two variables enables insight into both the degree of correlation and the phase shift in the variables. By computing the power spectrum of this lagged correlation common periods in the two data sets are revealed and to what degree these frequencies are present in the data sets. Correlation coefficients above 0.4 signify correlation. If there is a correlation, the phase can be found by looking at the shift in the periodic correlation. Finally, the power spectra show whether the 27-day and 11-year cycles are present in the wind. To determine whether solar irradiance or energetic particle precipitation is the cause of these cycles, seasonal variations will be examined. If $Y_{10.7}$ is the main contributor, the data is expected to correlate more in winter and summer compared to the yearly average. If, on the other hand, AP plays

the biggest part, the correlation should be increased in the summer and decreased in the winter compared to the yearly average.

2 Theory

2.1 The atmosphere

Encapsulating the earth is a thin layer of gas called the atmosphere. Protecting the earth from dangerous radiation from the sun, burning up thousands of meteors each day, giving humans air to breathe in, providing weather systems and heating the planet, the atmosphere is crucial for life on earth. In volume, the atmosphere is composed by 78% nitrogen (N_2), 21% oxygen (O_2), about 1% argon (Ar), 0.04% carbon dioxide (CO_2) and other minor constituents [9].

The atmosphere is divided into vertical layers delimited by changes in the sign of the temperature gradient. Closest to earth and on average 10 km up in the atmosphere is the troposphere. Heat is radiated from the earth and out of the troposphere, giving a negative temperature gradient in this layer. Above the troposphere extending to 50 km above the surface of the earth is the stratosphere. Most of the ozone is located here, therefore a common name for this region is the ozone layer. Due to absorption of solar UV radiation and chemical reactions with ozone releasing energy, the temperature gradient is positive. From about 50 km and up to 85 km is the mesosphere. The temperature is characterized by cooling due to radiation of heat and dynamic wave forcing from below, which lead to minimum temperatures varying between -120°C in the summer and -63°C during winter. The thermosphere extends from 85 km to 690 km above ground level. It is composed of the lightest gases oxygen, helium and hydrogen. Gas molecules absorb UV and x-ray radiation and dissociate into atomic species. The excess dissociation energy creates fast moving atoms whose velocity, characterized as a temperature, increases to as much as 1500 degrees Celsius [3]. The vertical structure of the temperature gradient in the atmosphere is presented in figure 1 [10].

The temperature in the atmosphere controls the concentration of many chemical species through temperature sensitivity on the reactions. Infrared radiative cooling by carbon dioxide and to some extent ozone and water is balanced with absorption of solar energy by O_3 and O_2 and water vapor [9], [11]. In the stratosphere and mesosphere, absorption of UV by molecular ozone is the most dominant heating factor. The penetration depth of solar radiation significantly alters the chemistry in the atmosphere [12]. UV, visible and near infra-red radiation emitted by the sun correspond to wavelengths between 0.1 and $4\,\mu$m, while the earth emits infra-red radiation with wavelengths between 4 and $100\,\mu$m.Infrared radiation emitted by the earth between 8 and 11 micrometers is not absorbed by the atmosphere and the band is called the atmospheric window [7], [9], [12].

The atmosphere is coupled through radiative processes, wave propagation and

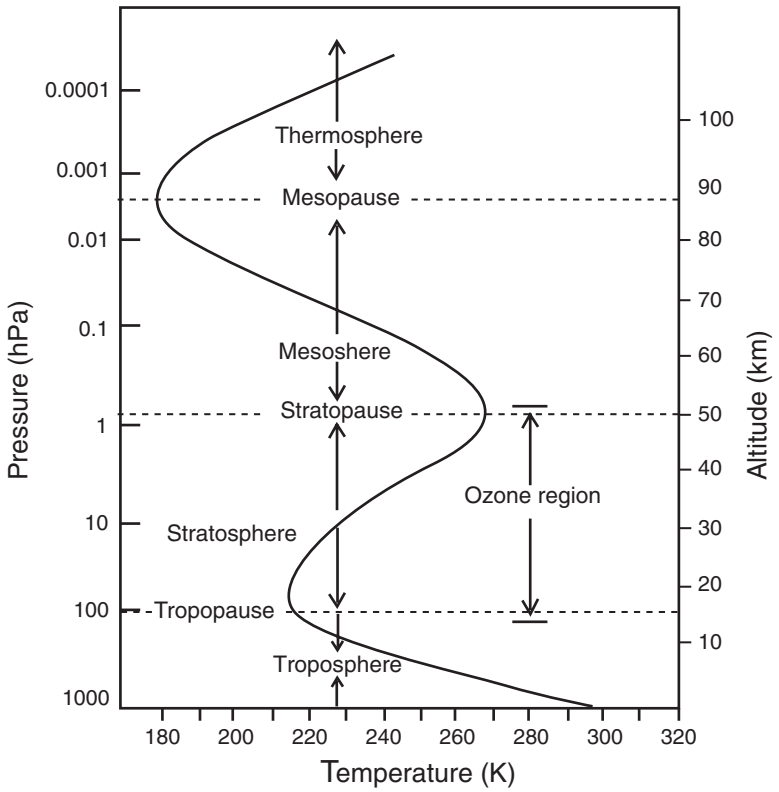

Figure 1: Figure of the vertical structure of the temperature gradient in the atmosphere with respect to altitude and pressure from [10]. The layers described in section 2.1, their pauses and the ozone region are marked in the figure.

mass exchange, according to Smith [1]. Haigh et al. [13] state that temperature variations may also cause changes in wind and weather systems. Stray [5] finds that the mesosphere-lower thermosphere is strongly influenced by the conditions in the underlying atmospheric layers.

2.2 Atmospheric circulation

During summer, the stratosphere above the summer pole is heated continuously for months due to the inclination of the earth. As a result, the temperature decreases from the stratospheric summer pole towards the equator, continuing to drop from the equator towards the cold, dark winter stratospheric pole. Globally, there is a net flow towards the winter pole on both hemispheres due to the pressure differences arising from the temperature variations. The Coriolis force turns the wind into strong westward wind in the summer stratosphere and eastward wind in the winter stratosphere such that the meridional component is very small.

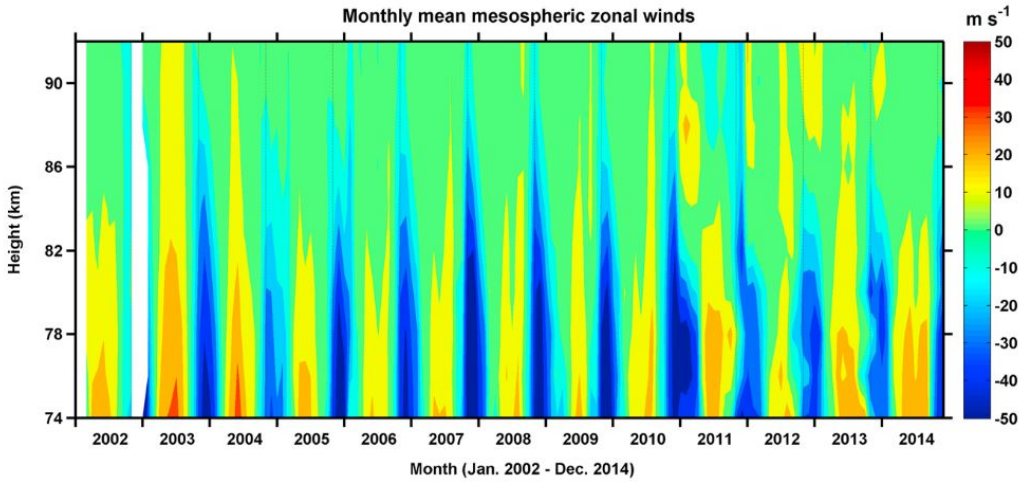

Figure 2: Figure of monthly mean mesospheric zonal winds from 75 to 95km, during 2002 through 2014 from [14].

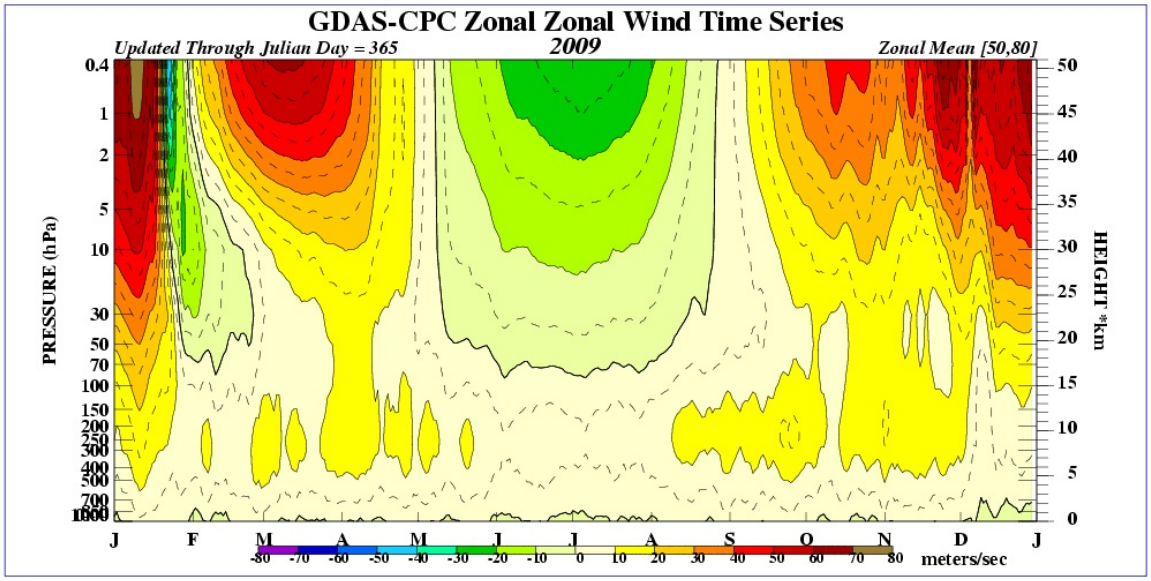

Figure 3: Zonal mean wind in 2009 from National Oceanic and Atmospheric Administration at altitudes ranging from 0 to 50 km at 50° north and 80° east [15]. There was a winter sudden stratospheric sudden warming in 2009.

In the mesosphere, radiatively driven winds, which go in the same direction as the ones in the stratosphere described above, compete with the drag force from gravity wave momentum deposition. The drag force rotates the mesospheric wind toward the winter pole and away from the summer pole, creating a decrease of zonal flow as shown in figure 2 and an increase of meridional flow.

Figure 3 depicts the mean zonal wind throughout 2009 at altitudes ranging from 0 to 50 km at 50° north and 80° east. In the stratosphere, there was westward flow during the summer in 2009 and eastward during winter, except for a brief reverse of this flow in January and February. That is a winter sudden stratospheric warming. These rather short-lived events add to the atmospheric variability that is not connected to solar activity, and thus represent a source of "geophysical noise" in this thesis.

2.3 Causes of mean wind variability

2.3.1 Atomspheric variation with solar irradiance

Chemistry and dynamics are of equal importance to the energy deposition in the MLT. The MLT is similar to the average atmosphere described in section 2.1, except for less water, lower density than the layers below and higher concentrations of ozone. Many reactions in the MLT are driven by solar radiation, hence imposes a diurnal

variation in the composition of chemical species [11], [12].

Radical oxygen (O) is the most important reactor in the upper part of the mesosphere and lower part of the thermosphere and is the main absorber of solar energy in the same region. Combined with molecular oxygen, radical oxygen forms ozone.

Energetic particle precipitation (EPP), described in section 2.5, controls the chemical structure starting at the upper stratosphere, the mesosphere and including the lower thermosphere. Electrons and protons ionize molecular oxygen and nitrogen which again react into nitric ($\mathrm{NOx} = \mathrm{N}, \mathrm{NO}, \mathrm{NO_2}$) and hydrogen oxides ($\mathrm{HOx} = \mathrm{H}, \mathrm{OH}, \mathrm{HO_2}$). NOx and HOx gases undergo catalytic reactions with ozone that reduce ozone concentrations. In combination with the central role of ozone for the energy in the atmosphere and the catalytic nature of these reactions, only slight changes in NOx and HOx gases may perturb the energy balance in the atmosphere considerably [12], [16].

Gravity waves (GW's), see section 2.3.2, are predominantly controlling the wind in the MLT on a large time and space scale basis by depositing momentum in the mesosphere. In the stratosphere, as stated in section 2.2, there is predominantly eastward wind during winter and westward wind during summer. Gravity waves are absorbed by the mean flow if the phase velocity is smaller than the wind velocity. Effectively, the stratosphere absorbs the eastward GW's in the winter and the westward GW's in the summer. Stronger wind in the stratosphere leads to more GW-filtering in the stratosphere. The remaining gravity waves continue to propagate upwards in the mesosphere, increasing exponentially in amplitude due to decreasing density higher in the atmosphere. Eventually, the GW's exceed the adiabatic lapse late, they are unstable and break. Due to the stratospheric filtering, westward momentum in the winter and eastward momentum in the summer is deposited in the MLT as the wave breaks. Induced by the wave breaking is a drag force, which in combination with the Coriolis force turns the wind in the mesosphere towards the winter pole establishing the meridional residual circulation from the summer pole to the winter pole. The drag force decreases or reverses the magnitude of the zonal wind and enhances the meridional wind. The effect of gravity wave filtering on the zonal winds are shown in figure 4. This, in turn, creates a convergence of air in the winter pole and causes downwelling and heating, while the dispersion of air at the summer pole causes upwelling and cooling.

2.3.2 Other variations of mean wind

There are other factors that create changes in the mean wind that may add variability that disguises the solar driven changes this work seeks to quantify. Some can be eliminated by averaging their effects over appropriate time intervals, and others will

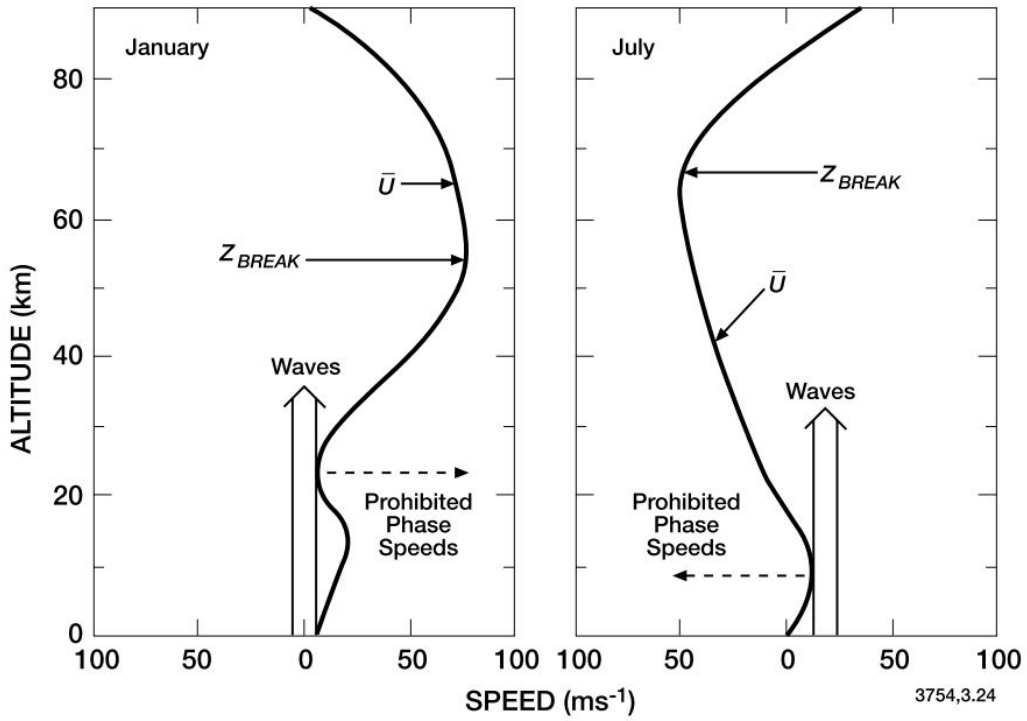

Figure 4: Visual representation of the mean zonal winds in the stratosphere from [12] with respect to altitude. Winter conditions are shown on the left panel and summer on the right. Prohibited phase speeds and breaking levels for mesospheric gravity waves are also presented.

add so called "geophysical noise" which are real variations not associated with the processes wished to study in this thesis. Briefly, some of these sources of variability are described here.

Pressure, temperature, velocity and density oscillating together is a phenomenon called gravity waves [7]. Obstructions like mountains or weather fronts force an air parcel in the troposphere upwards out of its equilibrium state. The parcel moves down to compensate for the displacement, however, inertia causes the parcel to continue oscillations up and down. Gravity waves propagate horizontally and vertically with a period between a few minutes and one day and with wavelengths from 10-1000 km [5], [7], [12].

Equivalent to tides in the ocean, there are also tidal variations in the atmosphere in temperature, pressure, density and winds. Migrating tides are driven by the sun, implying that the period is 24 hours or a fraction of 24 hours. Diurnal tide corresponds to 24 hour-period, semidiurnal tide corresponds to 12 hour-period and terdiurnal tide corresponds to 8 hour-period. In the troposphere, tides originate from heat changes, as water absorbs heat and from heat emission due to phase changes of water. Stratospheric ozone absorbs solar UV radiation resulting in increased heat in the stratosphere. After generation in the troposphere and stratosphere, tides propagate away from these areas. The density in the atmosphere decreases exponentially with height. Consequently, waves propagating upwards will increase exponentially in amplitude [1], [7]. Since these tides and gravity waves have periods less than one day, averaging data to daily means can be used to eliminate the variability they cause.

Planetary waves, also known as Rossby waves, are large-scale oscillating wind systems that travel around the earth. As the upper atmospheric zonal winds encounter high and low-pressure barriers induced by land-sea temperature differences in the lower atmosphere, they are deflected horizontally around them in a wave-like oscillation. Due to the variation of the Coriolis force with latitude, these global, wave-like patterns of high- and low-pressure move slowly westward in time, giving rise to what is termed planetary waves with periods between 2 and 20 days. Unfortunately, averaging data to daily means will not remove the effects of planetary waves, which remain a source of noise on a daily basis. However, longer, seasonal averages will reduce this noise.

Another wind phenomenon that affects the mean wind is stratospheric sudden warmings (SSW) which last from a couple of days to a few weeks [2]. They are formed as the eastward winter polar vortex is disturbed by the breaking of powerful planetary waves carrying westward momentum, causing a change of direction for the vortex. The strong vertical wind gradients caused by stratospheric sudden warmings can generate planetary waves in the mesosphere and lower thermosphere [1], [5]. In 2009 there was

a sudden stratospheric warming in the winter, which can be seen in figure 3. At the end of January and beginning of February, the wind is westward as opposed to the normally eastward winds during winter, like expected during a sudden stratospheric warming. The wind changes associated with SSW are not directly related to solar variability, and thus their effects will also add to the geophysical noise when looking at solar induced changes to the mean wind.

2.4 The sun

Our nearest star, the sun, is built up by a core with a strong magnetic field and an atmosphere surrounding it. The most abundant elements on the sun are hydrogen (92.1%) and helium (7.8%). The visible part of the sun is called the photosphere, which holds a temperature of 5780K. Surrounding the photosphere is a thin layer called the chronosphere, where the temperature is 10^4K. Even further out from the center of the sun is the corona, with temperatures as high as $2 \cdot 10^6$K and this ionizes most of the solar atmosphere into a mixture of ions and electrons called plasma. The hot plasma escapes the sun's gravity field because the particles have very high velocities and flow out beyond the earth. This constant stream of plasma is known as solar wind. As the solar wind interacts with the earth's magnetic field, plasma can be transferred, energized, and forms the basis for earth's radiation belts, called Van Allen belts, and auroras. These particles can enter the atmosphere and modify the chemistry and dynamics of the mesosphere and stratosphere [17].

2.5 Solar cycles

The sun follows an eleven-year periodic solar cycle, which it has done in historic timescales [18]. Solar phenomena such as sunspot number, solar intensity and energetic particle precipitation are periodic, and the solar dynamo is the source for all of them. Every eleven years, the magnetic field of the sun changes and flips direction. As the sun is spinning around its axis, charged particles follow this motion and create a magnetic field, just like a dynamo. The sun rotates faster at the equator than near the poles. The period varies between 25 days for the high-altitude regions and 30 days for low-altitude regions. Also, the magnetic fields follow this rotation. The magnetic field inside the sun coils up and can form magnetic loops that stretch out into the corona. The areas where these magnetic loops penetrate the surface of the photosphere are called sunspots, and the regions surrounding these spots emit more UV radiation than the rest of the photosphere. Most of the sunspots are located at mid-altitudes, rotating with a period of just above 27 days.

In proximity to sunspots, sudden explosions of energy called solar flares can occur.

These are sometimes combined with huge mass and radiation emissions called coronal mass ejections lasting about 10 minutes [19]. Electrons, protons and some heavier ions are ejected with an average speed of 600km/s, close to the speed of light. The magnetic field lines restrict the charged particles, which follow a curved trajectory while spiraling the field lines [17]. Electrons at high speed emit radio waves in addition to hard X-rays when they reach the lower solar atmosphere. Protons emit gamma rays as they ascent towards the chromosphere or photosphere. The energetic particles from one coronal mass ejection carry about 10^{25}Joule energy. Solar irradiance emitted by the sun follow the solar cycle, during solar maximum the sun emits more solar irradiance and during solar minimum the sun emits less. On the other hand, energetic particle precipitation maximizes when solar irradiance is increasing or decreasing.

The magnetic field of the sun is constantly changing, and every eleven years, it changes direction. The simultaneous events of zero magnetic field and a minimum number of sunspots mark the beginning of a new sunspot cycle. In the course of two such cycles, the magnetic poles are swapped back to their original positions, which marks one repetition of the approximately 22-year Hale cycle [18]. In the course of one solar cycle, an increasing number of sunspots appear at mid-latitudes, moving towards the equator while dying out [19]. During the time interval 1994 to 2016, the minima were in May 1996 and December 2008 and the maxima in March 2000 and April 2014 [20].

3 Materials and Methods

3.1 Wind in the MLT

3.1.1 The Super Dual Auroral Radar Network

The Super Dual Auroral Radar Network (SD) is a series of high-frequency upper-atmospheric radars. The network was founded to study plasma of electrically charged particles close to the earth, and its effect on the atmosphere and infrastructure such as communications [21]. In 2020 SD has more than 35 radars spread out on both hemispheres. SD is an international organization consisting of multiple universities and research institutions around the globe.

Meteor echoes appeared in the data from SD for the lowest altitudes at about 85 to 105 km. These were further developed by Hall et al. [22] to provide reliable measures of winds at 95 km in the mesosphere and lower thermosphere (MLT), using the least square method. When small meteors enter the atmosphere, they start to burn and leave an ionization trail behind them. This trail moves with the local wind. High-frequency signals from SD radars are reflected, and by measuring the phase-shift of the pulses in time, the wind in the line of sight can be calculated. In addition, the time the signal took to return gives the range of the echo. From the angle of the radar, the altitude of the meteor echo can be estimated. Combining multiple lines of sight at different azimuth angles gives a resulting meridional and zonal wind.

SD has given excellent results in studying dynamical processes in the atmosphere during the last 25 years. Not only successful in the study of plasma, but a wide range of magnetospheric and ionospheric phenomena [23]. In comparison between two different SD radars located in Saskatoon, Canada and Tromsø, Norway, Hussey et al. found that the meteor radar results agree well at heights of about 95km [24]. Comparing with other measuring techniques like very high-frequency radars in Kiruna, Sweden and the SD radar located in Finland, but measuring over Kiruna, Arnold et al. [25] found that these agree well. Arnold et al. also implied that this is valid for the other SD radars. The SD station at Halley, Antarctica, was compared to an imaging Doppler interferometer by Hibbins et al. [26]. These approximately co-located instruments correlate best at 90-95km height.

3.1.2 Mean wind data

This project utilizes hourly mean wind data from the station called Saskatoon, located in Canada at 52.16° north and -106.53° west [27]. The dataset spans the time between 1st of January 1994 and 31st of December 2016. The radar at Saskatoon is directed towards the north and contains 32 beams that span 16 degrees on each side

of the north. Consequentially it measures the meridional, north-south wind better than the zonal, east-west wind.

3.2 Solar indices

The sun emits radiation and charged particles. Solar irradiance describes the amount of electromagnetic radiation emitted by the sun hitting a square meter of the earth. Geomagnetic precipitation like charged electrons and protons enter the earth's atmosphere, where they react and disturb the environment. Excitation of oxygen and nitrogen by solar emitted particles is the origin of the auroras.

3.2.1 Solar irradiance and $Y_{10.7}$

Solar indices are a measure of the radiation flux intensity emitted by the sun that hits the earth. As the solar intensity flux emitted by the sun is known, it is possible to calculate the intensity absorbed by a specific area on earth. The sun emits energy of different wavelengths, some of which are absorbed in the atmosphere. Therefore the absorbed energy at a specific latitude and altitude may vary in height. In order to use an appropriate solar index in calculations, a number of different solar indices have been developed. In this thesis, the $Y_{10.7}$ index is used, which represents the solar irradiance deposited in the MLT.

In 2008 Bowman et al. published a new atmospheric density model called JB2008 [28]. This model includes a new semiannual variation equation, geomagnetic index and solar indices, the latter of particular interest.

The energy deposited in the mesosphere lower thermosphere is predominantly from X-rays, extreme ultraviolet (EUV) and Lyman-α radiation. X-rays and EUV are created in the corona both in rapidly changing solar flares and slowly varying bright, active regions on the sun and have a wavelength of $0.1 - 10$nm and up to 100nm, respectively. The energy in x-rays is deposited by ionizing and dissociating oxygen and nitrogen in the atmosphere. Lyman-α radiation is ultra-violet radiation from one of the emission lines of hydrogen, created in solar active regions on the sun in the chromosphere and the transition region. Dissociation of nitrogen oxide (NO) and reactions including water (H_2O) Lyman-α radiation deposits energy in the earth's atmosphere.

The $Y_{10.7}$ index used in this thesis has components of both solar flux, X_{10} and Lyman-α in the following relation

$$Y_{10.7} = F_{81norm}X_{10} + (1 - F_{81norm})L_{10},$$

in solar flux units (sfu = $10^{-22}\mathrm{Wm}^{-2}\mathrm{Hz}^{-1}$). Here, F_{81norm} is 81-day smoothed $F_{10.7}$ divided by its mean value, X_{10} is an index for x-ray radiation deposited in the mesosphere and lower thermosphere and L_{10} is Lyman-α radiation which origin from regions around sunspots [29].

3.2.2 Solar indices data

The European Space Agency (ESA) provides data for several solar indices. The Space Situational Awareness program was established to detect threats from space to life, infrastructure and property. In this project $Y_{10.7}$ index is used because it represents the energy deposited in the mesosphere-lower thermosphere on a daily basis, as opposed to $F_{10.7}$ which has been used traditionally. The dataset is from the 1st of January 1997 to the 12th of September 2020.

3.2.3 Energetic particle precipitation and AP

The solar cycle affects the energetic particle precipitation, or solar wind, reaching the earth. This precipitation induces geomagnetic storms and auroras. The flux of these particles tends to peak a few years after the solar UV and can be characterized by geomagnetic indices.

AP is a linear index aimed to give a measure of the planetary geomagnetic activity in the mid-latitudes in the atmosphere. K was introduced in 1938 and aimed to measure geomagnetic activity. It was a discontinuous variable describing the largest geomagnetic variation in one dimension of a three-dimensional reference system every three hours at a station. Due to diurnal and seasonal variations, Ks was developed to elude these variations and also to create a continuous variable. By averaging Ks over all the stations, the Kp index was formed, describing the planetary geomagnetic activity at mid-latitudes. Directly converted from the quasi-logarithmic Kp index, ap is a convenient, linear scale serving arithmetic purposes. AP is the average of eight three-hour values of ap, resulting in daily values [8].

3.2.4 Geomagnetic indices data

The AP index in this project is provided by National Oceanic and Atmospheric Administration (NOAA). NOAA is an U. S. Government agency that aims to understand and predict changes in climate, weather, oceans and coasts, while sharing this information with others. The organization offers reliable data for K, Kp and AP indices. Monthly averages for AP from January 1994 through December 2016 are used in this thesis [30].

3.3 Preliminary work

Following is a summary of the work executed on the data for wind and the solar index $Y_{10.7}$ in the pre-phase of this thesis, which was presented in the preliminary report. To avoid errors in the hourly data for the wind provided by SD, certain limitations were placed on them. The minimum number of data points each hour was set to 25 in order to achieve an acceptable signal-to-noise ratio. Wind speeds exceeding $\pm$150m/s were removed as outliers [5]. As the mean winds were found using the least-squares method, data points with standard deviation equal exactly zero were removed because the least square method did not converge. If the longitude deviated more than 1° from the station, measurements were removed as this represented a special, non-standard configuration of the radar. Removed values were replaced with NaNs (not a number). Then the hourly data were fitted using a mean wind plus sine waves at 48-, 24-, 12-, and 8-hours over a sliding 4-day window. This provides a 4-day smoothed daily mean wind, where the effects of tides and the strong 2-day planetary wave have been removed. Finally, the 40-day averaged climatology was subtracted from the data to get the anomaly used in this project.

The dataset for $Y_{10.7}$ spanned the time from 1st of January 1997 to 12th of September 2020. Data for $F_{10.7}$ was available for the remaining period from 1994 to 1997. The relationship between $Y_{10.7}$ and $F_{10.7}$ is well described by a polynomial of second degree. Using available data for both solar indices, the fitted polynomial provided the missing values for $Y_{10.7}$.

3.4 Correlation

Correlation describes whether or not there exists a relationship between two variables. There are multiple ways for this to happen, for example they may be co-dependent on a third unknown variable or one of them depends on the other. The simplest way of correlation is a linear relationship between the variables x and y, such that y = a + rx, where a and r are constants and $r \in [-1, 1]$. In the linear case, r is given by [31]

$$r = \frac{N \sum x_i y_i - \sum x_i \sum y_i}{N \sum x_i^2 - (\sum x_i)^2}.$$

If $0 < r < 0.4$ there is weak or no correlation between x and y, if $0.4 < r < 0.7$, there is moderate correlation and $r > 0.7$ implies strong correlation. Positive r means a positive correlation, and if r is negative, there is a negative correlation. r^2 is the percentage of points within $\pm 1\sigma$ of the linear fit.

If the processes connecting the two variables are shifted in time, introducing a lag is helpful to discover this correlation. The lagged correlation reveals trends that

are common for the two variables but not necessarily in phase. The lag at which the lagged correlation peaks gives the phase shift between the signals, and the height of the peak the degree of linear correlation at that lag.

It is not possible to determine which variable is leading which without knowledge about the physical process at hand. A useful supplement to the cross-correlation is the cross-spectrum described in section 3.5 providing the period or frequencies of the repetitive nature of the correlation.

3.5 Power spectral analysis

Power spectra represent the signal power of the frequencies present in a signal. When analyzing the correlation function, a concentrated power spectrum indicates a predictable signal, one that correlates. In many cases, the Fast Fourier Transform (FFT) is sufficiently accurate, even though other methods provide better frequency resolution. The fundamental frequency is the frequency where the signal repeats itself. Infinite signals give continuous spectra because the fundamental frequency, $f_0 = 1/T_0$, approaches zero and T_0 approaches infinity.

The Cooley-Tukey algorithm calculates the discrete Fourier transform (DFT) using the FFT. The DFT is given by equation (1) where $x(m)$ is a discrete-time signal with N samples and $X(k)$ is the discrete Fourier transform with N uniformly spaced samples [32].

$$X(k) = \sum_{m=0}^{N-1} x(m)e^{-j(2\pi/N)mk}, \qquad k = 0, ..., N-1 \tag{1}$$

Other steps were performed after the Cooley-Tukey algorithm to avoid certain problems. A Hamming filter diminishes the samples close to the edges of the sample. Figure 5 pictures a Hamming window with 1000 samples in time-domain. The filter is applied to decrease the presence of high frequencies in the power spectrum due to abrupt changes at the beginning and end of the time series. Frequencies with corresponding periods close to or higher than N are unreliable and uninteresting in this project and are removed by subtracting a mean from the data.

The sample was padded with zeros to increase the frequency resolution. It was appropriate with $6N$, rounded up to the next power of two, additional zeros. The one-dimensional N-point discrete FFT was calculated at this point. Finally, the power spectrum was obtained by taking the square of the absolute value of the FFT.

There are certain limitations to this course of action. The uncertainty principle in the FFT limits the resolution of frequency and period in the following manner:

$$\Delta T \Delta f = 1.$$

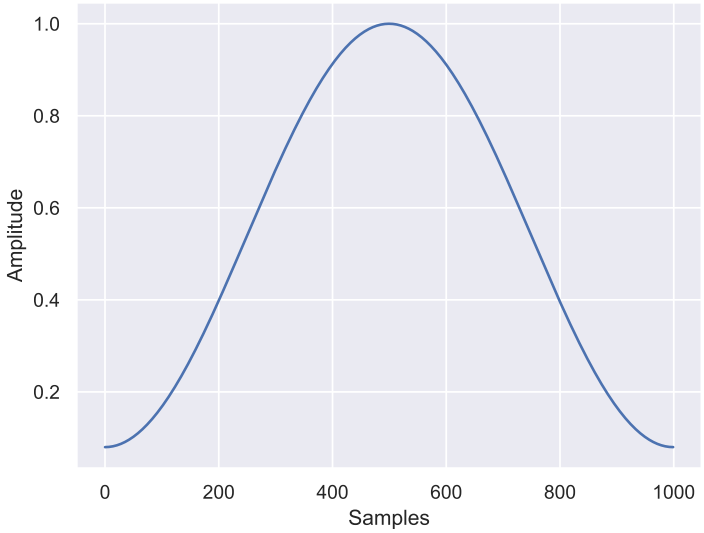

Figure 5: Hamming window with 1000 samples in time-domain.

It is not possible to reconstruct the original waveform with the power spectrum due to the lack of information about the phase of the various frequencies. Finally, the ability to compute the Fourier transform rely on finite energy of the signal.

4 Results

4.1 Solar rotational cycle in the mean mesospheric wind

In this section, the influence of the rotational solar cycle on the daily mean wind in the MLT is explored by use of lagged correlation between the daily mean mesospheric wind and the daily solar index $Y_{10.7}$. The lagged cross-correlation was performed on subsets of a year of daily data with up to 60 days lag. The number of lags is called N. Pearson's correlation coefficient, r, with 95% confidence interval is plotted with respect to N. The sun leads the wind at negative lags.

The lagged cross-correlation for meridional wind in 2008 is exhibited in figure 6 and for 2014 in figure 8. There was a solar minimum in December 2008 and a solar maximum in April 2014. The correlation coefficient from 2008 varies between -0.4 and 0.13 in a periodic manner. The confidence interval deviates with ± 0.1. In figure 8, r oscillates between approximately ± 0.25 together with the confidence interval, which deviates about 0.1 from r. The first peak or valley to the left of zero lag is at -1 in 2014 and -2 days in 2008, implying that the effect of the solar radiation on the wind comes 1 and 2 days after the radiation has entered the atmosphere.

The corresponding cross-spectrum from figure 6 is shown in figure 7. The frequency with the highest amplitude is 1/26 days. The peak is fairly slim and much higher than the smaller ones. The cross-spectrum of the cross-correlation from figure 8 is presented in figure 9. The cross-spectrum between the winds and the $Y_{10.7}$ index show a strong peak near 29 days. The peaks indicate that both time series, mean wind and $Y_{10.7}$, have a phase-coherent oscillation at that period.

Table 1 present several properties of the 60-day lagged correlation between $Y_{10.7}$ and the meridional and zonal wind and the corresponding cross-spectra from 1994 through 2016. Variables with subscript V refer to meridional and U to zonal wind. $< Y_{10.7} >$ is the yearly average of $Y_{10.7}$. r_{cc} is the amplitude of the first peak to the left of zero lag which can indicate how similar the two time series are. τ is the lag for that peak, signifying the phase between the two oscillations. T_{max} is the maximum period in the cross spectra, indicating the period of the strongest cyclical variation common to the time series correlated. A_{ps} is the cross spectral amplitude of the maximum period, which is proportional to the magnitude of the average cross-correlation across all lags.

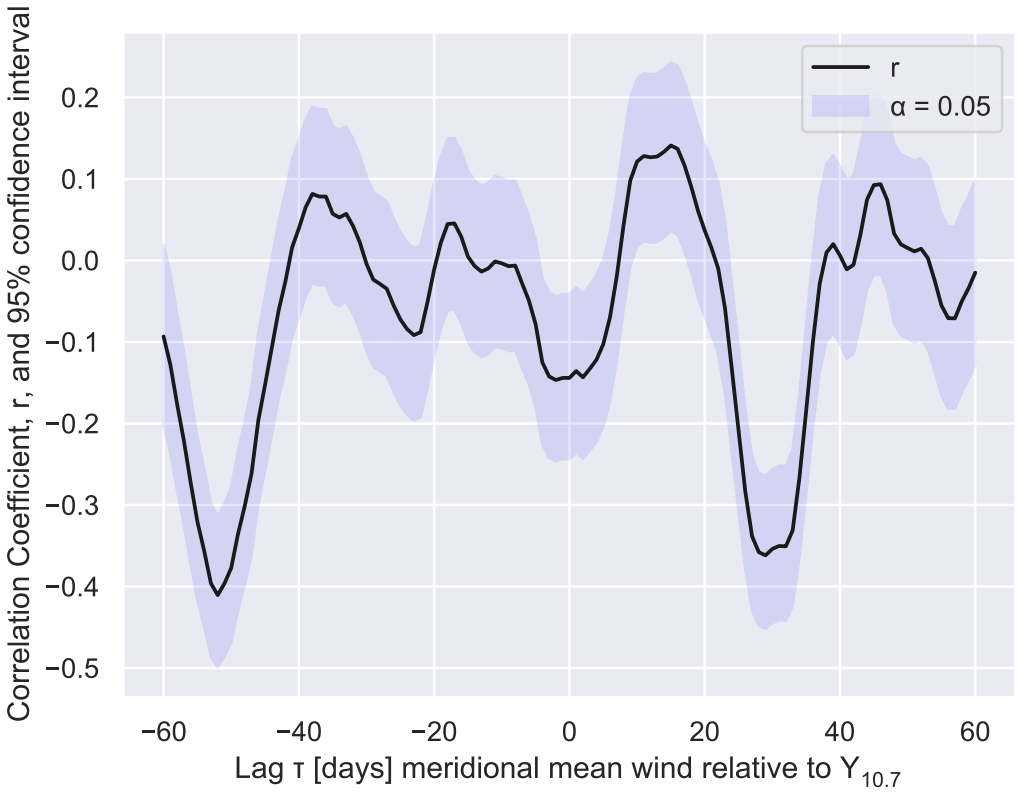

Figure 6: 60-day lagged cross-correlation between daily meridional mean wind and $Y_{10.7}$ from 2008 with 95% confidence interval. Negative values refer to days $Y_{10.7}$ leads the wind.

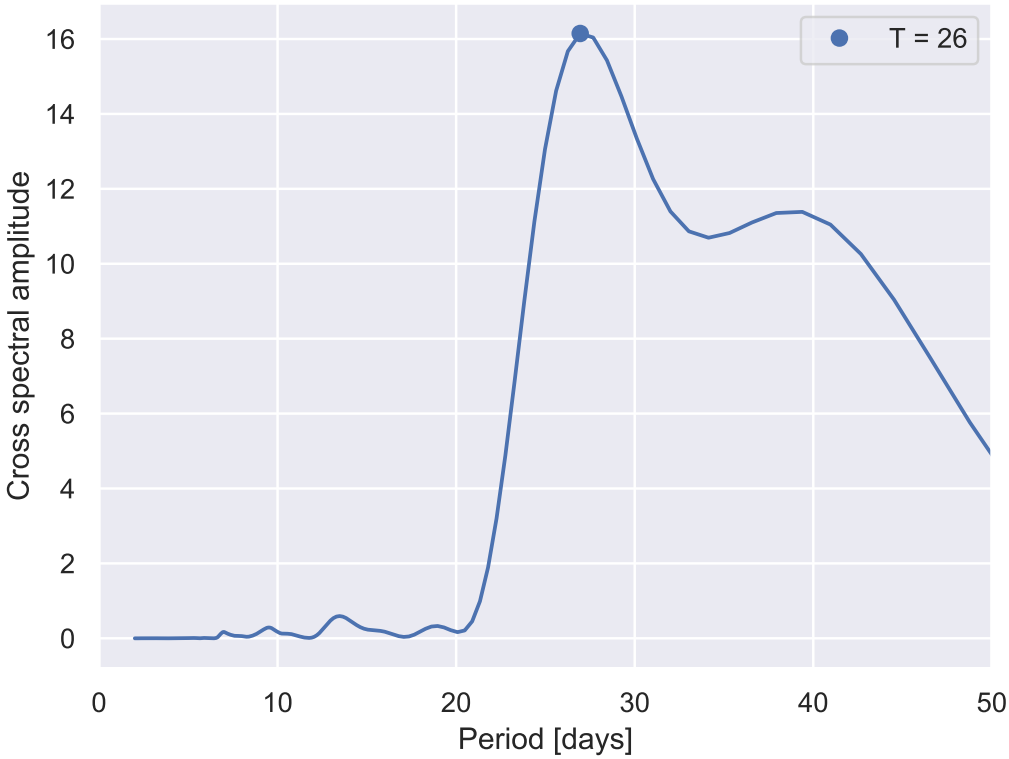

Figure 7: Cross-spectra of the cross-correlation in figure 6. The period with the highest amplitude is marked with a blue point.

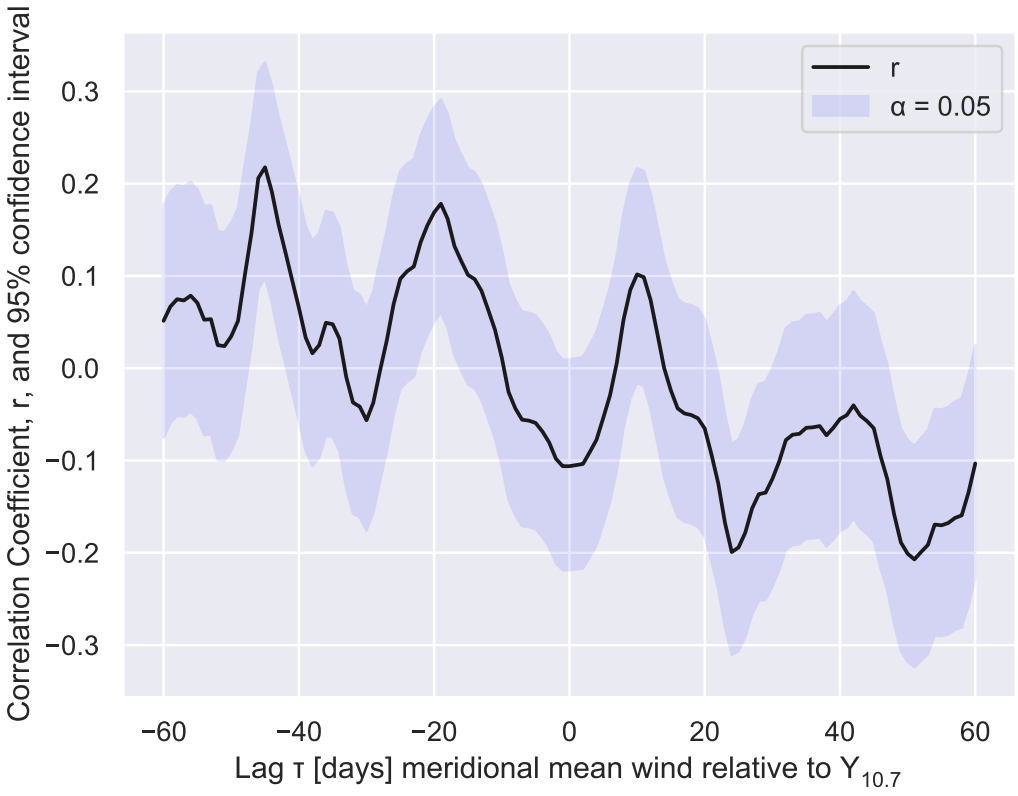

Figure 8: 60-day lagged cross-correlation between daily meridional mean wind and $Y_{10.7}$ from 2014 with 95% confidence interval. Negative values refer to days $Y_{10.7}$ leads the wind.

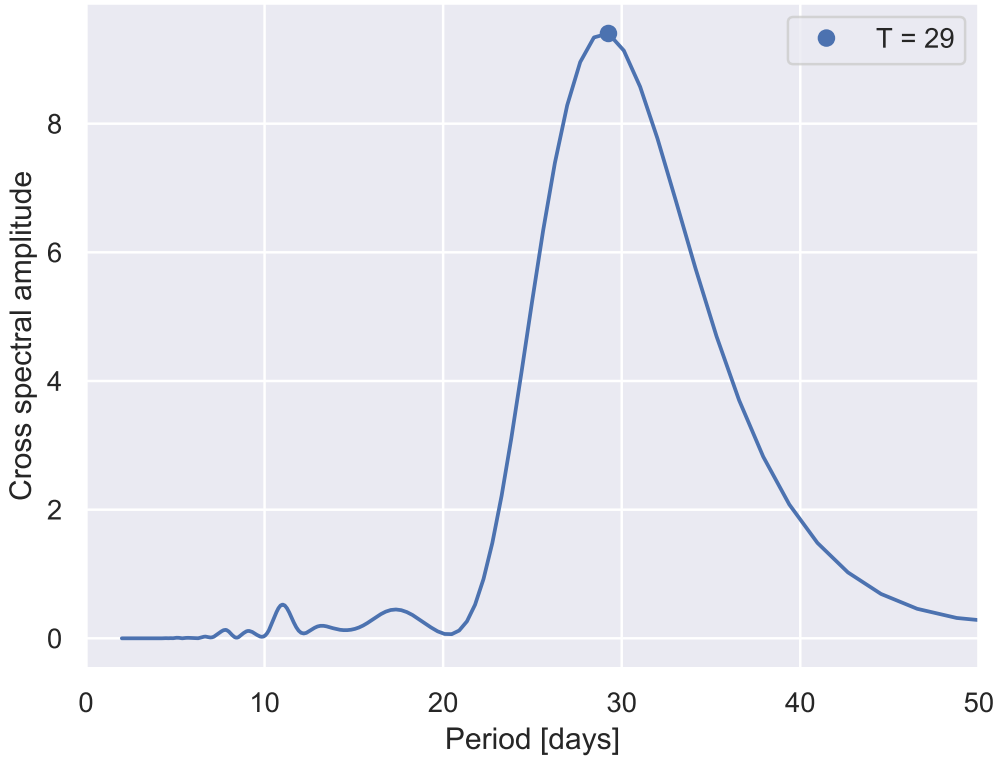

Figure 9: Cross-spectra of the cross-correlation in figure 8. The period with the highest amplitude is marked with a blue point.

Table 1: Variables from the yearly 60-day lagged cross-correlations and cross-spectra for the meridional and zonal wind. Variables with subscript V refer to meridional and U to zonal wind. $< Y_{10.7} >$ is the yearly average of $Y_{10.7}$ in $10^{-22}\mathrm{Wm}^{-2}\mathrm{Hz}^{-1}$. r_{cc} is the amplitude of the first peak to the left of zero lag and τ the lag for that peak in days. T_{max} is the maximum period between 20 and 36 days in the cross spectra in days. A_{ps} is the cross spectral amplitude of the maximum period.

Year	$< Y_{10.7} >$	$r_{cc,V}$	$r_{cc,U}$	τ_V	τ_U	$T_{max,V}$	$T_{max,U}$	$A_{ps,V}$	$A_{ps,U}$
1994	89.0	-0.15	-0.10	-3	-7	27	29	8.0	1.9
1995	78.5	0.03	0.18	-5	-4	26	34	5.4	1.6
1996	71.6	0.16	0.39	-8	-1	27	22	7.0	5.4
1997	83.0	0.22	0.11	-9	-1	31	29	1.6	4.1
1998	126.8	-0.18	0.35	-6	-3	26	26	2.7	3.7
1999	151.9	-0.10	-0.11	-2	-1	31	30	5.2	9.9
2000	165.2	0.11	0.26	-9	-6	24	26	3.0	23.6
2001	163.9	-0.22	-0.71	-1	16	30	28	4.7	1.8
2002	170.9	0.23	-0.19	-12	-1	28	32	9.0	8.4
2003	137.4	0.26	0.25	-7	-20	27	32	37.6	4.6
2004	115.9	0.04	0.14	-4	-13	25	34	9.3	3.3
2005	98.6	-0.34	-0.27	-11	-10	26	26	65.1	16.1
2006	79.9	0.24	-0.05	-16	-3	33	22	33.3	2.5
2007	64.1	-0.14	0.17	-4	-1	23	28	5.6	5.2
2008	58.0	-0.15	0.05	-2	-4	26	25	16.1	16.6
2009	58.6	0.07	-0.13	-12	-11	27	27	7.5	9.4
2010	85.5	0.17	-0.05	-1	-3	27	27	13.0	4.6
2011	119.9	-0.11	-0.22	-6	-2	26	22	2.5	2.6
2012	123.8	-0.07	0.14	-11	-7	28	25	40.1	18.2
2013	120.3	-0.35	0.27	-3	-14	34	29	12.4	22.4
2014	133.4	-0.11	-0.27	-1	-8	29	26	9.4	8.8
2015	129.3	-0.05	-0.19	-3	-9	26	26	4.7	9.3
2016	95.7	0.47	-0.45	-3	-6	28	28	16.6	14.0

4.2 Year-to-year variations of the rotational cycle

The cross-spectral amplitudes for both the meridional and zonal wind given in table 1 are cross-correlated with the yearly average of the solar index $Y_{10.7}$, also in table 1, in figure 10. The solar index leads the cross-spectral amplitudes at negative lags. The cross-correlation varies between ± 0.5 for both cases implying moderate correlation accounting for a lag between the solar index and the winds. However, if one were to do a straight, 0-lag cross-correlation, there would only be a very weak 0.2 and -0.1 correlation. At negative five years, where $Y_{10.7}$ leads the wind, the meridional

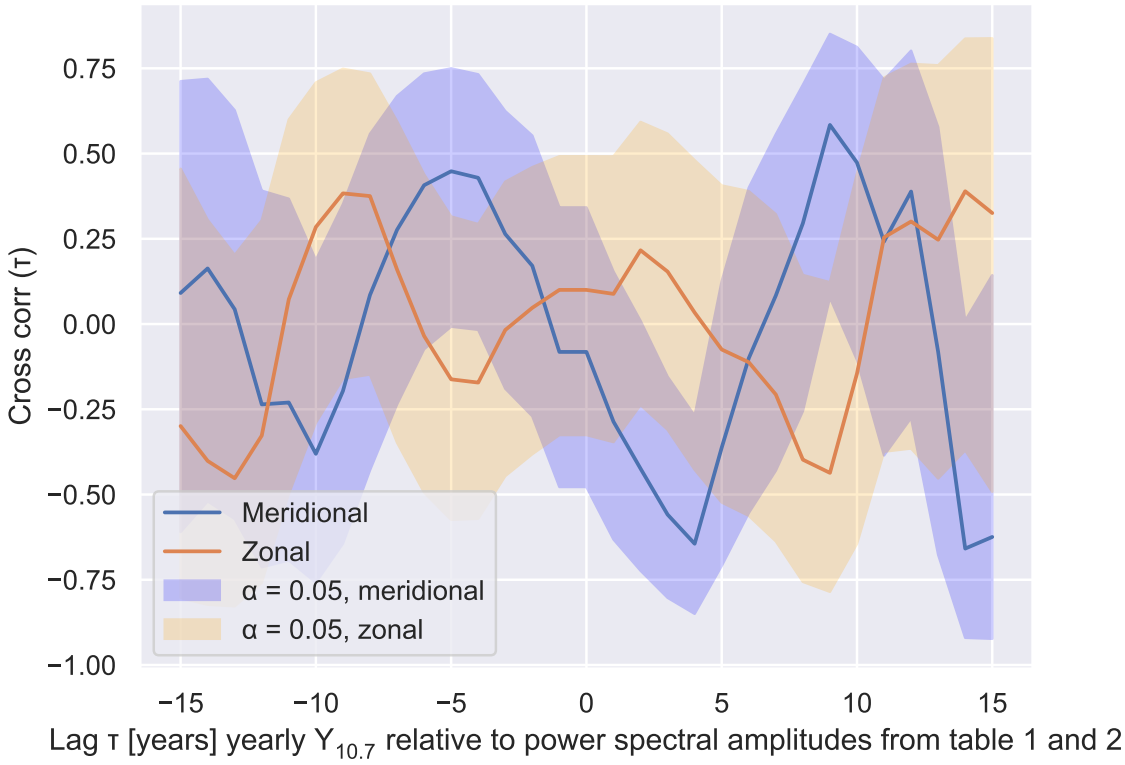

Figure 10: Cross-correlation of the yearly cross spectral amplitudes from the rotational cycle (table 1) and yearly averages of $Y_{10.7}$. The solar index leads the cross spectral amplitudes at negative lags.

power spectral amplitudes have their maximum correlation with $Y_{10.7}$, while the zonal power spectral amplitudes have their maximum anti-correlation at approximately the same lag. The 180° phase-shift between meridional and zonal wind seems to be the case for the rest of the correlation as well. The confidence intervals belonging to the correlation coefficients deviate with about ±0.3-0.4.

The cross-power spectrum of the cross-correlation between the zonal cross spectral amplitudes and yearly averages of $Y_{10.7}$ is presented in figure 11. The cross spectrum for meridional cross spectral amplitudes correlated with $Y_{10.7}$ is in figure 19 Appendix A.1 because of the similarity to figure 11. Both cross-spectra peak at a period of 13 years. The cross-spectrum indicates a phase-coherent oscillation at 13 years is present in the solar index as well as each of the zonal and meridional winds.

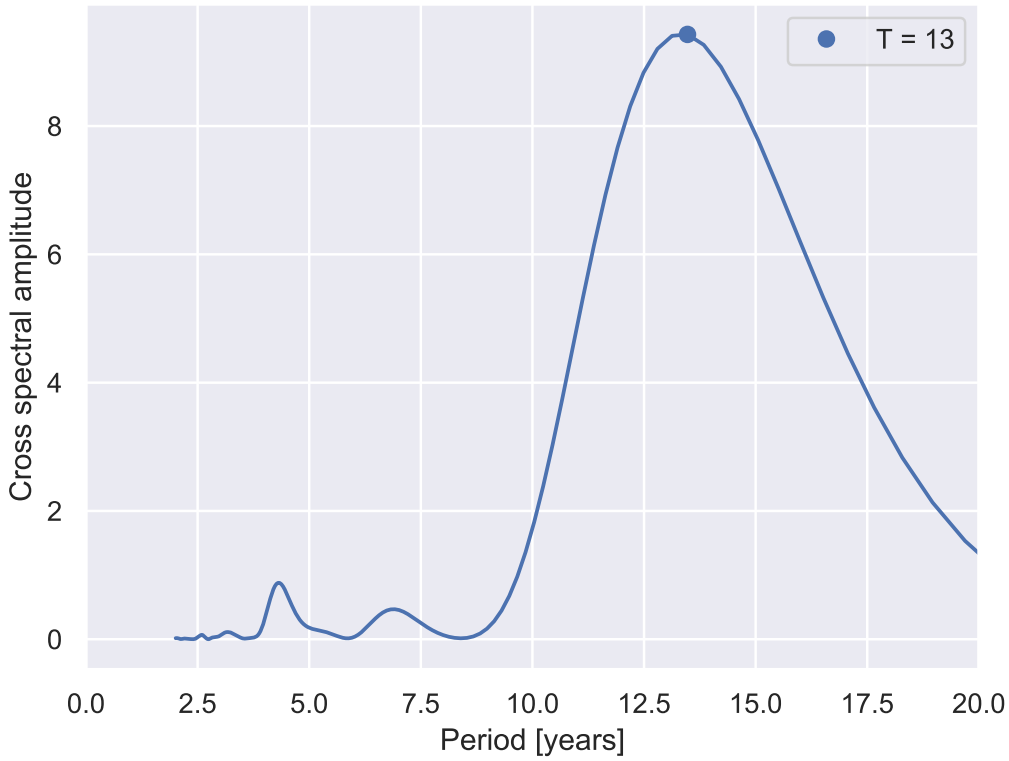

Figure 11: Cross spectrum of the lagged correlation between the yearly maximal zonal cross spectral amplitudes from figure 10 and $Y_{10.7}$. The period with the highest amplitude is marked with a blue point.

4.3 Sunspot cycle in the mean mesospheric wind

This section focuses on long-term variations in the solar index $Y_{10.7}$, the geomagnetic index AP and meridional and zonal mean wind, aimed at finding the 11-year solar cycle. The yearly average is mean wind averaged over a full year. The data labeled winter are averaged over December one year and January and February the following year. The summer data are averaged over May, June and July. Table 2 gives the yearly averaged quantities to be analyzed.

Table 2: The yearly average, $< V >$ and $< U >$, is mean wind averaged over a full year in m/s. U is zonal wind and V is meridional wind. The data labeled $< V_{win} >$ and $< U_{win} >$ in m/s are averaged over December one year and January and February the following year. The summer data in $< V_{sum} >$ and $< U_{sum} >$ in m/s are averaged over May, June and July. $< Y_{10.7} >$ is the yearly average of $Y_{10.7}$ in $10^{-22}\mathrm{Wm}^{-2}\mathrm{Hz}^{-1}$. NaNs refer to not a number, see section 3.3.

Year	$< Y_{10.7} >$	$< V >$	$< V_{sum} >$	$< V_{win} >$	$< U >$	$< U_{sum} >$	$< U_{win} >$
1994	89.0	0.21	1.06	-0.44	0.42	-9.45	-2.64
1995	78.5	-0.34	1.23	-1.17	-0.71	-9.78	-1.40
1996	71.6	-0.66	-0.11	-2.98	-0.55	2.50	0.61
1997	83.0	-0.03	1.25	-0.29	0.86	4.44	0.15
1998	126.8	-0.02	-2.07	3.90	0.12	1.83	0.13
1999	151.9	2.22	2.70	3.31	2.16	-2.79	9.91
2000	165.2	-1.43	-2.81	-2.74	1.99	1.70	0.24
2001	163.9	0.22	-0.66	0.99	0.36	0.68	4.14
2002	170.9	0.19	-1.13	3.06	0.29	3.06	-3.81
2003	137.4	-0.05	-0.70	0.91	0.54	-1.74	-1.89
2004	115.9	-0.34	1.28	0.98	1.49	-1.03	9.15
2005	98.6	-0.11	0.49	-2.15	-2.99	1.49	-3.10
2006	79.9	1.16	-0.04	4.63	1.14	3.56	0.88
2007	64.1	0.95	1.34	0.38	-0.82	1.96	-1.87
2008	58.0	-0.34	0.54	-0.28	-1.40	1.10	0.99
2009	58.6	-0.73	-0.71	-1.26	0.17	0.63	0.94
2010	85.5	1.11	0.75	-1.12	-3.00	1.16	-3.38
2011	119.9	-0.61	0.51	-2.15	-0.52	1.35	-4.17
2012	123.8	1.07	0.65	2.09	0.03	-0.87	1.18
2013	120.3	-0.63	-0.32	-0.69	2.29	1.93	5.34
2014	133.4	-0.22	-0.24	-3.83	-0.96	1.61	1.31
2015	129.3	-0.93	-1.85	-1.29	-0.37	3.45	-1.42
2016	95.7	-0.63	NaN	2.29	-4.68	NaN	-7.17

4.3.1 19-year lagged correlation between yearly averages of mean wind and $Y_{10.7}$

Table 3 presents some results from the lagged correlation of different yearly averages of meridional and zonal wind and $Y_{10.7}$. r_{cc} is the amplitude of the first peak to the left of zero lag in the cross-correlation, which can indicate how similar the two time series are. τ is the lag for that peak, signifying the phase between the two oscillations. T_{max} is the maximum period in the cross spectra, indicating the period of the strongest cyclical variation common to the time series correlated. A_{ps} is the cross spectral amplitude of the maximum period, which is proportional to the magnitude of the average cross-correlation across all lags.

Figure 12 depicts the lagged cross-correlation between yearly averages; full year, winter and summer, of the meridional wind and $Y_{10.7}$. Looking at the full year, one can observe some positive correlation with the $Y_{10.7}$ leading by close to a solar cycle. However, there is little evidence of an 11-year oscillation in the data. On the other hand, separating the wind into winter and summer seasons reveals that each lagged correlation has a strong cyclical behavior. However, the winter and summer seasons are about 180° out of phase. The winter winds show a broad maximum of correlation or about 0.25, with $Y_{10.7}$ leading by 2 to 3 years. At the same time, the summer winds show a narrow anti-correlation of about -0.4 with $Y_{10.7}$ leading by zero to one year. Taking the winds averaged over the full year shows virtually no correlation during this time. Confidence intervals deviate on average about ± 0.3 from r.

In figure 14 correlation between yearly averages of a full year, winter and summer zonal wind is correlated with $Y_{10.7}$. All three cases peak at around zero years lag, implying the same phase. The full year correlates better, at $r = 0.4$, than the winter and summer average with $r = 0.25$ and $r = 0.1$, respectively. The 95% confidence intervals deviate with about ± 0.3 from r.

The cross-spectra for the meridional yearly averages and $Y_{10.7}$ is presented for the yearly average in figure 13(a), summer in 13(b) and winter in 13(c). Surprisingly, the yearly average has a weak maximum in its cross spectral amplitude at a period of 11 years, indicating that the yearly average wind and $Y_{10.7}$ both oscillate with 11 years. The summer average and $Y_{10.7}$ oscillate together near the same frequency, 1/14 years. The winter average has a small peak in the cross spectrum at nine years period. The cross spectral amplitudes at these peaks are presented in table 3.

The cross spectra of cross-correlations in figure 14 between $Y_{10.7}$ and the yearly averaged zonal mean wind and the zonal summer and the zonal winter averages winds are in shown in figure 15(a), 15(b) and 15(c), respectively. In contrast to the meridional winds, the cross-correlation of all three of the zonal wind averages oscillates in phase as seen in figure 14. The yearly average of the mean zonal wind

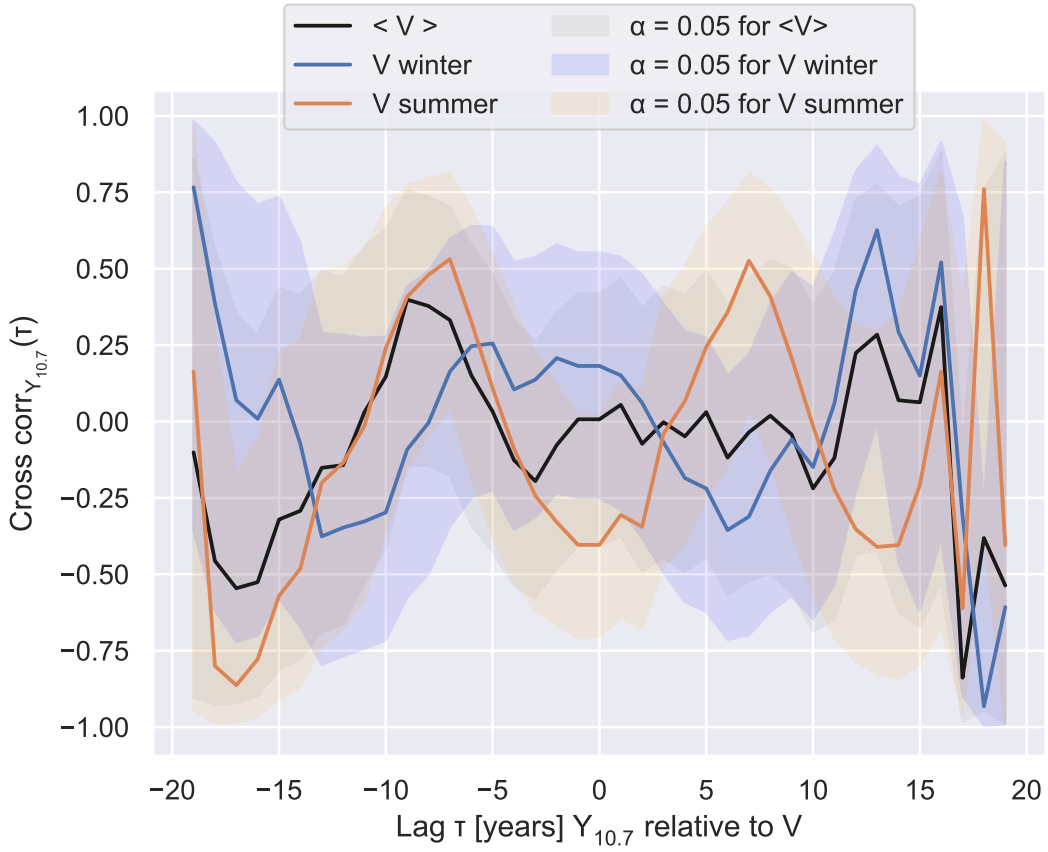

Figure 12: Cross-correlation with 95% confidence interval between yearly averages of $Y_{10.7}$ and meridional wind averaged over full years in black, summer meridional wind in orange and winter meridional wind in blue. Negative lags refer to years the solar index leads the wind.

peaks at 12 years, while the summer peaks at nine years, lastly, the winter peaks at 13 years. The peaks imply phase-coherent oscillations between zonal wind and $Y_{10.7}$ at the periods. Table 3 shows the corresponding cross-spectral amplitudes at these periods.

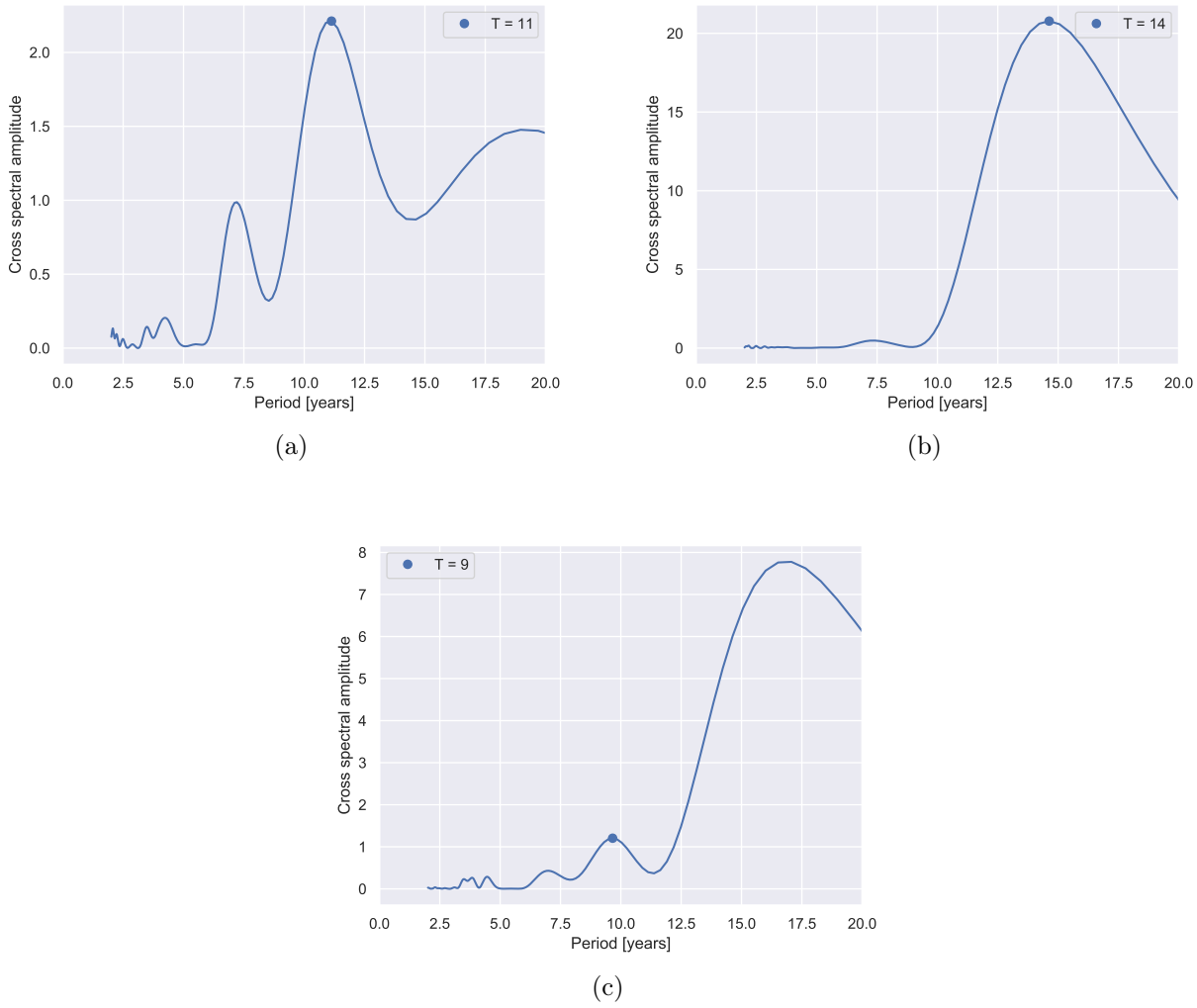

Figure 13: Cross spectral amplitude for the cross-correlation between yearly averages of $Y_{10.7}$ and (a) mean meridional wind, (b) summer meridional wind and (c) winter meridional wind. The local maxima near eleven years are marked with blue points.

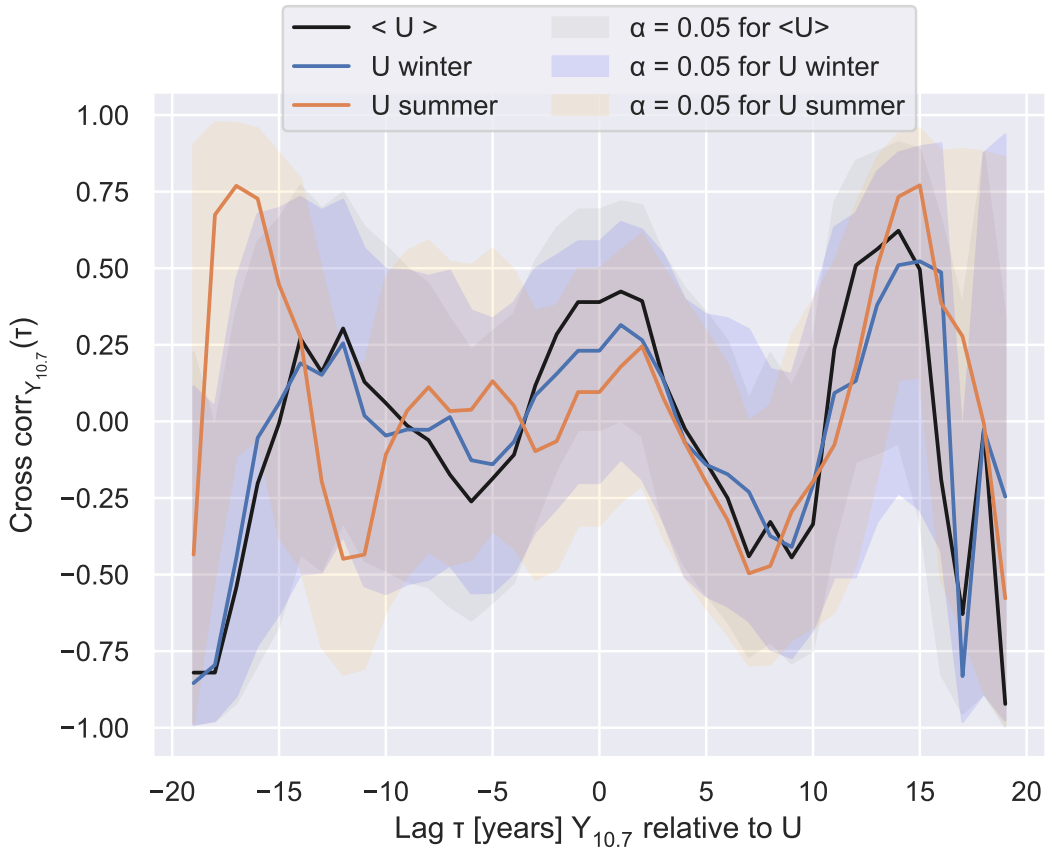

Figure 14: Cross-correlation with 95% confidence interval between yearly averages of $Y_{10.7}$ and zonal wind averaged over full years in black, summer zonal wind in orange and winter zonal wind in blue. Negative lags refer to years the solar index leads the wind.

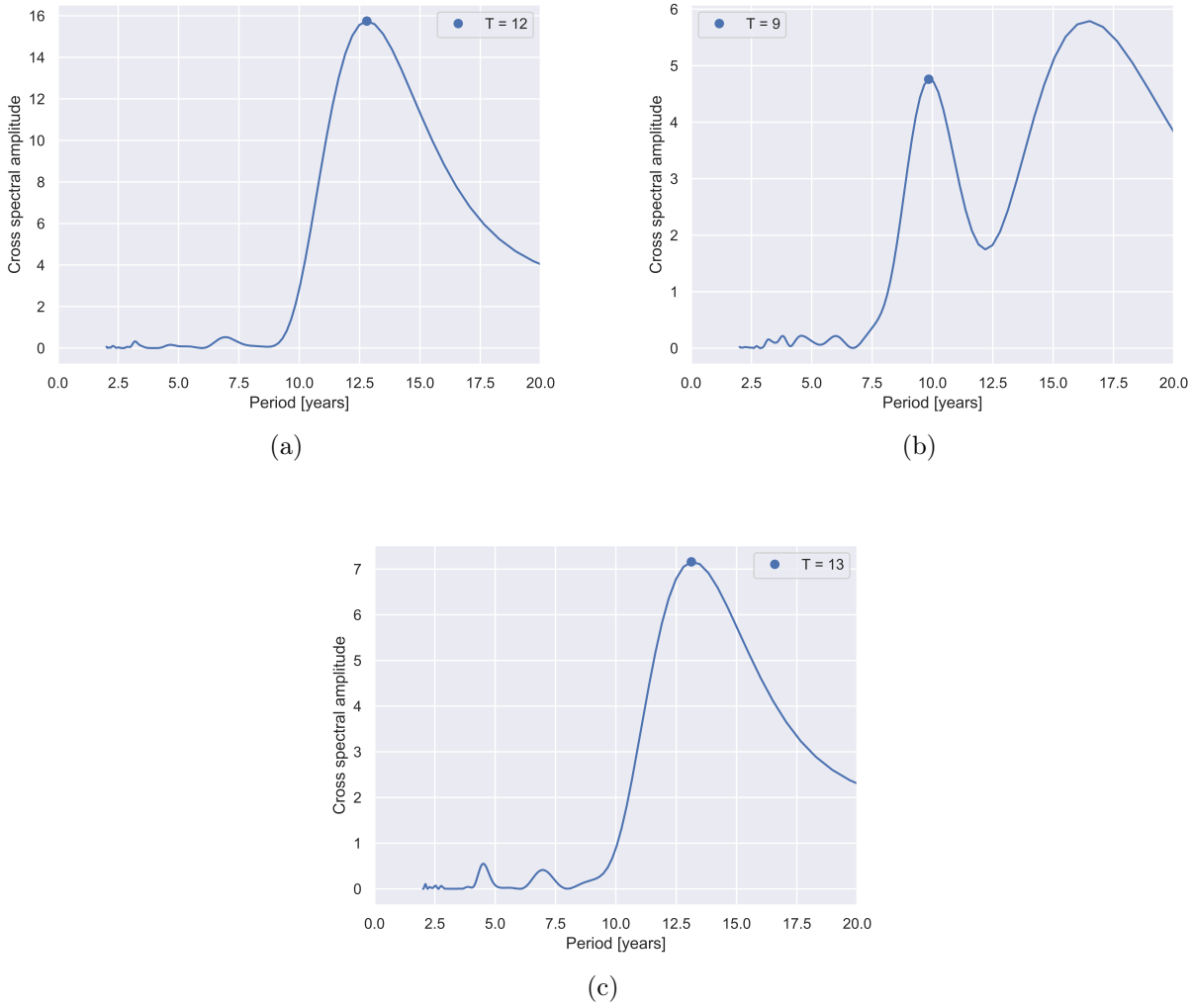

Figure 15: Cross spectral amplitude for the cross-correlation between yearly averages of $Y_{10.7}$ and (a) mean zonal wind, (b) summer zonal wind and (c) winter zonal wind. The local maxima near eleven years are marked with blue points.

Table 3: Some parameters from the lagged correlation between V and U averaged over a full year, winter and summer and $Y_{10.7}$. r_{cc} is the amplitude of the first peak to the left of zero lag and τ the lag for that peak in years. T_{max} is the maximum period in the cross spectra in years close to 11 years. A_{ps} is the cross spectral amplitude of the maximum period.

	r_{cc}	τ	$A_{ps(T_{max})}$	T_{max}
V full year	-0.20	-3	2.2	11.1
V summer	-0.41	0	20.8	14.6
V winter	0.20	-2	1.2	9.7
U full year	-0.25	-6	15.7	12.8
U summer	-0.11	-3	4.8	9.8
U winter	-0.14	-5	7.2	13.1

4.3.2 Solar irradiance or precipitation

The $Y_{10.7}$ and AP both vary with the solar cycle. Figure 16 aims to illustrate the similarities between the two variables to determine whether it is useful to do lagged correlation between yearly averages of wind and AP. The power spectrum of yearly averages of $Y_{10.7}$ and AP is shown in figure 16(a) and 16(b), respectively. Both power spectra have a peak at around ten years and smaller peaks at six and five years. For AP, the ten-year peak is a bit smoothed out due to the short distance to the big peak to the right of it.

The cross-correlation between yearly averages of $Y_{10.7}$ and AP is seen in figure 16(c) and corresponding cross-spectrum in figure 16(d). The indices are highly correlated, ranging between $r = \pm 0.75$. AP is shifted relative to $Y_{10.7}$ with a couple of years. In the cross-spectrum, the peak at 13 years period is the most prominent, which implies a common oscillation every 13 years for both AP and $Y_{10.7}$.

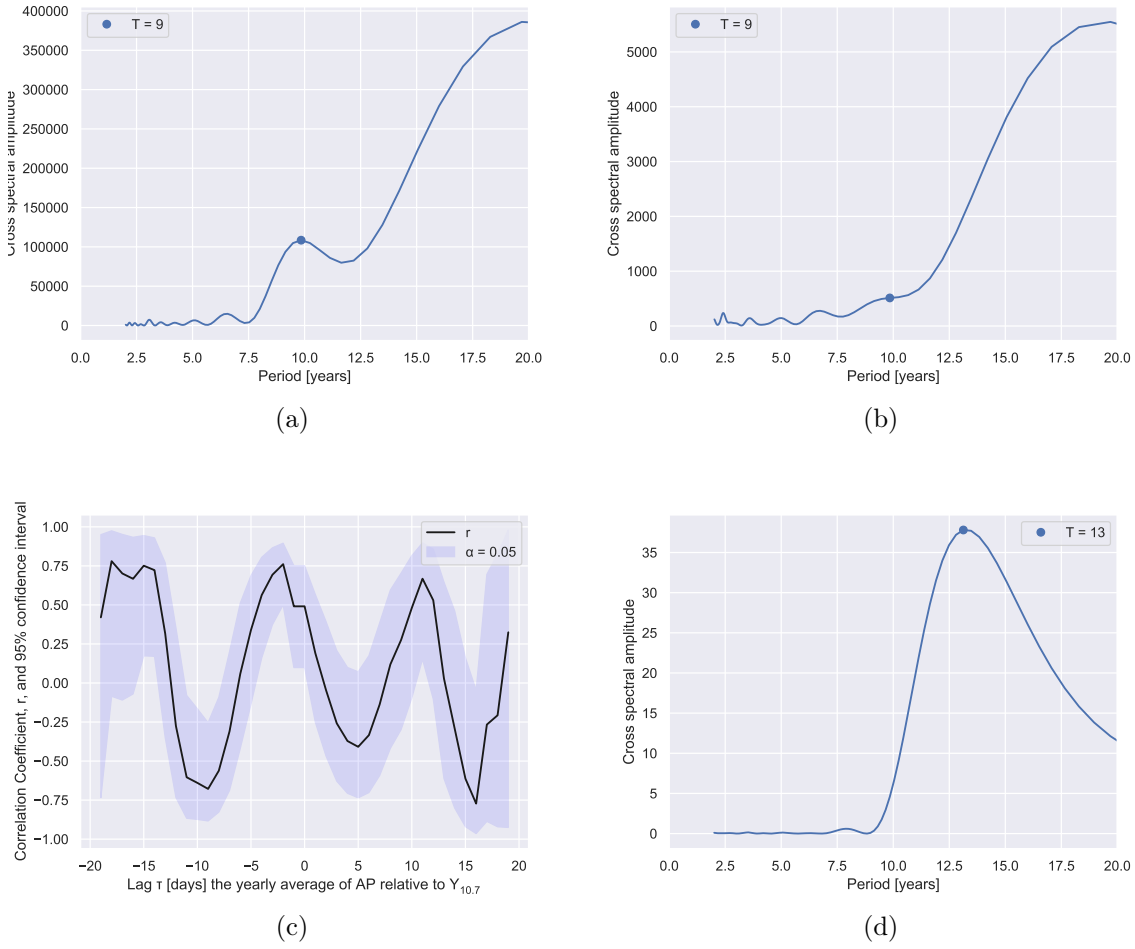

Figure 16: Power spectra of the yearly averages of (a) $Y_{10.7}$, (b) AP and (c) lagged cross correlation between AP and $Y_{10.7}$ and corresponding (d) cross-spectra of the two variables. The local maxima near eleven years are marked with blue points.

5 Discussion

5.1 Rotational solar cycle in the mean mesospheric wind

Variations of wind on time scales of the solar rotation period are examined in this section. Figure 6 and 8 shows the lagged correlation between the mean meridional mesospheric wind and $Y_{10.7}$ in 2008 and 2014, which is low, but significant. The correlation amplitudes of the first peak to the left of zero years lag in the correlation between mean meridional and zonal wind and $Y_{10.7}$ can be viewed in table 3. The correlation coefficients are mostly distributed between $\pm 0.1 - 0.3$, which is low. There are many other phenomena affecting the mean wind in the MLT, thus it is expected to find a weak correlation. In addition, the amplitudes of the mesospheric winds are relatively small compared to f.ex. the stratospheric winds. When looking at the rotational cycle, subsets of one year of daily values were used. Daily values vary a lot more than longer time averages, making it difficult to determine the true correlation. For example, planetary waves with periods between two and twenty days or impulsive events like sudden stratospheric warmings act independently from the solar irradiance and may disturb the mean wind. Even though tides and gravity waves should be averaged out when converting to daily values, waves in the stratosphere change the filtering of gravity-wave momentum reaching the mesosphere, thus can influence the wind. The gravity wave filtering functions as a drag force on the zonal wind in the MLT, which successively turns the wind. Often, the absolute value of the zonal wind is diminished, while the meridional wind is enhanced.

The first peak or valley to the left of zero days lag is at a couple of days negative lag for the meridional mean wind in 2008 and 2014. Table 3 show the phase shift between the meridional and zonal wind and $Y_{10.7}$ from 1994 through 2016. Meridional peaks and troughs are mostly shifted by two to nine days, while zonal peaks are mostly shifted by less than eight days. Winds arising from thermal radiation only lag the solar radiation by a few hours, while ozone in the stratosphere takes about seven days to heat up and induce the gravity wave filtering effect on the gravity waves reaching the mesosphere. If the variations in the MLT as caused by changes in the stratospheric gravity wave filtering, the expected delay would be 6-10 days [33]. The outliers of that interval can be explained by inaccurate measurements of the shift or geophysical noise.

In table 1 the period of the maximum cross-spectral amplitude around 27 days

are presented for the lagged correlation between meridional and zonal mean wind and $Y_{10.7}$. The periods correspond well with the solar rotational period, which varies between 25 and 30 days. These results are biased because of the selection interval between 20 and 36 days, but cross-spectra from most years had a local maximum in this interval. Figure 17 and 18 in appendix A.1 demonstrate that. The cross-correlation between meridional mean wind and $Y_{10.7}$ in figure 6 (2008) and 8 (2014) show periodic tendencies, confirming the strong implication that the mean wind is affected by the 27-day solar cycle in the solar irradiance.The number of sunspots visible on the photosphere increases during the solar cycle, making it harder to distinguish the effects of the individual sunspots. In 2008 there is a broad peak in the power spectra maximizing at 40 days, see figure 7. This may result from several sunspots following each other such that it looks like one sunspot with a longer period.

5.2 Yearly variations of the rotational cycle

Power spectral amplitudes of the about 27-day peaks and yearly averages of $Y_{10.7}$ from table 1 are cross-correlated in figure 10. r maximizes at ± 0.6, corresponding to moderate correlation. The cross spectral amplitudes are proportional to the average cross-correlation coefficient over all lags.

The meridional and zonal cross-spectral amplitudes are out of phase, which can be seen from the correlation with $Y_{10.7}$ in figure 10. The zonal correlation coefficient has a trough at -5 years lag, while the meridional correlation coefficient peaks at the same lag. Gravity wave filtering described in section 2.3.1 leads to an increase of meridional wind on the one hand and a decrease of zonal wind on the other. Therefore a phase shift between meridional and zonal wind is expected. The peak at -5 years lag implies that it takes five years for the solar irradiance to manifest changes in the mean wind in the MLT.

The cross-spectrum from the correlation between yearly averages of $Y_{10.7}$ and the power spectral amplitudes in table 1 peak at 13 years, see figure 19 and 11. Between 1994 and 2016, the time between two solar maxima and two solar minima was 12 (1996 to 2008) and 14 (2000 to 2014) years, on average 13 years. This corresponds well and supports the hypothesis that changes in solar irradiance affect the mean wind in the MLT. This suggests that the degree of correlation between mean wind in the MLT and the 27-day cycle in solar irradiance on a yearly basis varies with the 11-year solar cycle.

5.3 The sunspot cycle

Assuming the wind in the MLT is driven by temperature and pressure differences due to variation in the irradiance, and there is no dynamics, the mesospheric wind is expected to behave like the atmospheric circulation described in section 2.2. U is expected to be positive in the winter and negative in the summer in the northern hemisphere. The amplitude of V is very small because the wind is geostrophic, but if it has any amplitude at all, it is expected to be positive in the winter and negative in the summer. However, gravity waves alter the dynamics in the mesosphere. In wintertime, the zonal stratospheric wind increases as $Y_{10.7}$ increases, thus more eastward GW's are absorbed by the stratosphere. Westward momentum reaches the MLT and deposits westward momentum, which turns the eastward mesospheric winds westward and northward. An increase in $Y_{10.7}$ should give anti-correlation with zonal wind and correlation with meridional wind during winter. In the summer, zonal stratospheric winds become more westward with an increase in $Y_{10.7}$. Hence, eastward momentum is deposited in the MLT, turning the westward and slightly southward wind in the MLT eastward and southward. To sum up, the zonal winds are expected to correlate with $Y_{10.7}$ in the summer, while the meridional winds are expected to anti-correlate.

The atmospheric circulation in the stratosphere and the MLT if there were no dynamics, is positive in the winter and negative in the summer like described in section 2.2. Hence, the yearly average, which is the sum of the whole year of the mean wind, might not have that much of an amplitude at all. Thus, extracting winter and summer months will probably provide much larger variability from year to year. The separation gives insight into both the amplitude of the summer and winter wind and the relative difference between them and the average of an entire year.

Figure 12 and 14 present the lagged correlation between yearly averages of $Y_{10.7}$, mean wind, summer average and winter average for the meridional and zonal wind, respectively. At zero lag, the meridional wind correlates in the winter and anti-correlates in the summer, as expected from GW filtering. The zonal wind correlates both summer and winter, however, the winter wind was expected to anti-correlate. Figure 2 shows that the westward summer zonal flow reaches up to above 90 km altitude, while the eastward flow during winter is nearly 0 above 85 km. It appears that gravity waves have already reversed the wind westward and the winter winds show summer behaviour. As dynamics turns the wind winter zonal wind go from westward to eastward and northward, hence the impact of dynamics for the zonal wind is positive and also the correlation.

In figure 12 summer and winter correlations are in opposite phase. This can be explained by the gravity wave filtering, which decreases the zonal wind and increases

the meridional. Both the summer average, winter average and yearly average of the mean zonal wind in figure 14 have local maxima at around zero years lag. It is reasonable to believe that the solar irradiance effects act within the same year, the results confirm that.

There is no physical reason that the wind leads the sun, therefore only the negative lags are interesting. Near the ends of the correlation, only a few points overlap, thus these results must be used carefully. Another aspect of these results is the length of the data sets, which is only 23 years, making it hard to find long-term trends like the 22-year Hale cycle, see section 2.5. Longer data sets would improve the reliability of the results.

The cross spectra in figure 13 and 15 are reasonable because they peak at 10 to 14 years, which corresponds well with the solar cycles in the relevant period of time. The broad peaks at 16 and 17 years in figure 13(c) and 15(b) might be there because of variation between one solar cycle and the next. Considering the length of the data set, these longer periods should not be taken into account because they probably represent noise or variations of the strength of the solar cycle.

5.3.1 AP

The power spectrum of yearly averages of $Y_{10.7}$ and AP is presented in figure 16(a) and 16(b). Both indices peak at nine years, with some smaller peaks at shorter periods and a broad peak at higher periods with the highest amplitude. The broad peak in figure 16(a) and 16(b) to the right are there probably because of inclination of the data set. As these peaks peak close to the length of the data set, they should not be considered. In the cross spectra between the yearly averages of AP and $Y_{10.7}$, 13 years appear to be the shared period with the highest amplitude. This is the same as the cross spectra for $Y_{10.7}$ and various yearly averages of wind. The similarity between the indices makes it impossible to determine whether AP contributes to the mean wind in the MLT with the methods used in this thesis.

Averages of AP and $Y_{10.7}$ correlate with correlation coefficient up to $r = \pm 0.75$, which is moderate correlation. The correlation between $Y_{10.7}$ and averages of wind is relatively low compared to the correlation between AP and $Y_{10.7}$, hence, imposing difficulties in separating the effects from EPP and solar irradiance on the mean wind in the MLT. The correlation coefficient in figure 16(c) peaks at about three years lag, which is reasonable because AP peaks when $Y_{10.7}$ increases or decreases.

In Appendix A.1 figure 20 and 22 the correlation between yearly averages of AP and meridional and zonal mean wind, summer and winter averages. Based on the lag between AP and $Y_{10.7}$, there is no way saying whether AP or $Y_{10.7}$ correlates better with the mean winds in the MLT. The cross spectra in figure 21 and 23 show peaks

at 4, 8, 9, 10, 13 and 14 years where most of the spectra have multiple peaks. One could argue that there is a solar cycle in AP and the mean mesospheric wind, but the results are unclear. In section 2.5 it is explained how both AP and $Y_{10.7}$ depend on the solar cycle. Therefore it is expected for them to correlate and difficult to distinguish between the two using the method of cross-correlation and cross spectra. Also, semiannual variation and high noise levels in AP make it harder to distinguish the effects. Because of the same periodic trends and moderate correlation, modelling is a tool to declare AP or $Y_{10.7}$ as the main driver in the MLT. By removing the lower latitude chain of SD radars, the area where the wind is affected by the auroral effect would cut out. Then a comparison between lower and higher latitudes would reveal whether solar irradiance and particles is the main driver of mean wind in the MLT.

6 Conclusion

There is a weak, yet significant correlation between the mean wind in the MLT and $Y_{10.7}$, which is a measure of the solar irradiance power deposited in the MLT. The correlation varies periodically with both the rotational and sunspot cycle of the sun. Gravity wave filtering by radiatively driven stratospheric winds is probably decreasing the strength of the wind in the MLT, hence also the correlation. Other phenomena like sudden stratospheric warmings and physical processes spending different amounts of time affecting the wind probably weaken the correlation. Therefore I conclude that the mean wind in the MLT is driven, at least partly and perhaps indirectly through stratospheric gravity-wave filtering, by solar irradiance. To improve the reliability of these results, longer data sets should be used.

On the question of whether the geomagnetic activity affects the mean wind in the MLT, I cannot exclude the auroral effect as a driver of the MLT. The methods used in this thesis revealed similarity in the variations of AP and $Y_{10.7}$, but are not sufficient in answering the question. Modelling is necessary to determine if EPP-driven mechanisms are consistent with the cross-correlation. However, such an analysis is beyond the scope of this thesis which was focused on identifying if any relationship existed. Future work can focus on the mechanisms behind this coupling.

Bibliography

[1] A. K. Smith, "Interactions between the lower, middle and upper atmosphere," *Space Sci. Rev.*, vol. 168, no. 1-4, pp. 1–21, Jun. 2012.

[2] R. A. Vincent, (2015, December), "The dynamics of the mesosphere and lower thermosphere: a brief review," *Prog. in Earth and Planet*, vol. 2, no. 1, [Online]. Available: `https://link.springer.com/article/10.1186/s40645-015-0035-8`.

[3] D. Boudreau (2012, Oct. 9), *National geographic society.* [Online]. Available: `https://www.nationalgeographic.org/encyclopedia/atmosphere/`, (accessed: 5.10.2020).

[4] K. Hamilton, "The Role of the Stratosphere in Tropospheric Climate Variability and Climate Change," *Newsletter of the International Pacific Research Center*, vol. 2, no. 1, pp. 8–11, Jun. 2002.

[5] N. Stray, "Planetary waves in the northern MLT: Vertical coupling and effects," Ph.D. dissertation, Dept. of Phys., Trondheim, 2015.

[6] R. J. De Wit, R. E. Hibbins, P. J. Espy, and E. A. Hennum, "Coupling in the middle atmosphere related to the 2013 major sudden stratospheric warming," *Ann. Geophys.*, vol. 33, no. 3, pp. 309–319, Mar. 2015.

[7] D. G. Andrews, *An introduction to atmospheric physics*, 2nd ed. Cambridge: Cambridge University Press, 2010.

[8] G. Rostoker, "Geomagnetic indices," *Rev. geophys.*, vol. 10, no. 4, pp. 67–100, Nov. 1972.

[9] F. K. Lutgens and E. J. Tarbuck, *The atmosphere : an introduction to meteorology*, 8th ed. Upper Saddle River, N.J: Prentice Hall, 2001.

[10] K. Mohanakumar, *Stratosphere Troposphere Interactions*, 1st ed. Dordrecht: Springer, 2008.

[11] J. M. Plane, W. Feng, and E. C. Dawkins, "The Mesosphere and Metals: Chemistry and Changes," *Chem. Rev.*, vol. 115, no. 10, pp. 4497–4541, Mar. 2015.

[12] S. Brasseur G. P. Solomon, *Aeronomy of the Middle Atmosphere*, 3rd ed. Dordrecht: Springer, 2005.

[13] J. D. Haigh and M. Blackburn, "Solar influences on dynamical coupling between the stratosphere and troposphere," *Space Sci. Rev.*, vol. 125, no. 1-4, pp. 331–344, Feb. 2006.

[14] N. Venkateswara Rao, P. J. Espy, R. E. Hibbins, D. C. Fritts, and A. J. Kavanagh, "Observational evidence of the influence of Antarctic stratospheric ozone variability on middle atmosphere dynamics," *Geophysical Research Letters*, vol. 42, no. 19, pp. 7853–7859, 2015, ISSN: 19448007. DOI: 10.1002/2015GL065432.

[15] NOAA. (2010). "Stratosphere-troposphere monitoring," [Online]. Available: https://www.cpc.ncep.noaa.gov/products/stratosphere/strat-trop/gif_files/time_pres_UGRD_MEAN_ALL_NH_2009.gif.

[16] M. Sinnhuber, H. Nieder, and N. Wieters, "Energetic Particle Precipitation and the Chemistry of the Mesosphere/Lower Thermosphere," *Surv. Geophys.*, vol. 33, no. 6, pp. 1281–1334, Nov. 2012.

[17] K. R. Lang, *The sun from space*, 2nd ed. Berlin: Springer, 2009.

[18] A. Balogh, H. Hudson, K. Petrovay, and R. Steiger, *The Solar Activity Cycle : Physical Causes and Consequences*. New York: Springer, 2015.

[19] R. A. Greenwald et al, "Darn/superdarn: A global view of the dynamics of high-latitude convection," *Space Sci. Rev.*, vol. 71, no. 1-4, pp. 761–796, Feb. 1995.

[20] S. C. Chapman, N. W. Watkins, and E. Tindale, "Reproducible Aspects of the Climate of Space Weather Over the Last Five Solar Cycles," *Space Weather*, vol. 16, no. 8, pp. 1128–1142, Jul. 2018.

[21] SuperDARN Canada. (2008). "What is superdarn?" [Online]. Available: https://superdarn.ca/about.

[22] G. E. Hall, J. W. MacDougall, D. R. Mooecroft, J.-P. St.-Maurice, A. H. Manson, and C. E. Meek, "Super dual auroral radar network observations of meteor echoes," *J. Geophys. Res.*, vol. 102, no. A7, pp. 14 603–14 614, Jul. 1997.

[23] G. Chisham, M. Lester, S. E. Milan, M. P. Freeman, W. A. Bristow, A. Grocott, K. A. McWilliams, J. M. Ruohoniemi, T. K. Yeoman, P. L. Dyson, R. A. Greenwald, T. Kikuchi, M. Pinnock, J. P. Rash, N. Sato, G. J. Sofko, J. P. Villain, and A. D. Walker, "A decade of the Super Dual Auroral Radar Network (SuperDARN): Scientific achievements, new techniques and future directions," *Surv. Geophys.*, vol. 28, no. 1, pp. 33–109, May 2007.

[24] G. C. Hussey, C. E. Meek, D. André, A. H. Manson, G. J. Sofko, and C. M. Hall, "A comparison of Northern Hemisphere winds using SuperDARN meteor trail and MF radar wind measurements," *J. Geophys. Res. Atmos.*, vol. 105, no. D14, pp. 18 053–18 066, Jul. 2000.

[25] N. F. Arnold, P. A. Cook, T. R. Robinson, M. Lester, P. J. Chapman, and N. Mitchell, "Comparison of D-region Doppler drift winds measured by the superDARN Finland HF radar over an annual cycle using the Kiruna VHF meteor radar," *Ann. Geophys.*, vol. 21, no. 10, pp. 2073–2082, Feb. 2003.

[26] R. E. Hibbins and M. J. Jarvis, "A long-term comparison of wind and tide measurements in the upper mesosphere recorded with an imaging Doppler interferometer and SuperDARN radar at Halley, Antarctica," *Atmospheric Chem. Phys.*, vol. 8, no. 5, pp. 1367–1376, Mar. 2008.

[27] SuperDARN Canada (2008), *Radar lookup table.* [Online]. Available: `https://superdarn.ca/radar-info`.

[28] B. R. Bowman, W. K. Tobiska, F. A. Marcos, C. Y. Huang, C. S. Lin, and W. J. Burke, *A new empirical thermospheric density model JB2008 using new solar and geomagnetic indices*, In: *AIAA/AAS Astrodynamics Specialist Conference*, Honolulu, Hawaii, 2008.

[29] W. K. Tobiska and S. E. Technologies, *The solar and geomagnetic inputs into the JB2008 thermospheric density model for use by CIRA08 and ISO 14222*, Jun. 2010. [Online]. Available: `https://www.spacenvironment.net/SpaceWxPubs.html`.

[30] NOAA. (2021). "About our agency," [Online]. Available: `https://www.noaa.gov/about-our-agency`.

[31] P. R. Bevington and D. K. Robinson, *Data reduction and error analysis for the physical sciences*, 3rd ed. Boston, Mass: McGraw-Hill, 2003.

[32] S. V. Vaseghi, *Advanced Digital Signal Processing and Noise Reduction*, 2nd ed. John Wiley Sons Ltd, 2000.

[33] D. F. Strobel, "Parameterization of the thermal relaxation rate in the stratosphere," *J. Geophys. Res.*, vol. 84, no. C5, pp. 2469–2470, May 1979.

A Appendix

A.1 Additional figures

The power spectra for the 60-day lagged correlation of subsets of one year between the meridional and zonal mean wind and $Y_{10.7}$ from 1994 to 2016 are shown in figure 17 and 18, respectively. To get a clear view, the years with maximum power spectral amplitude below five ranging between periods between 23 and 36 days are put in the lower plots.

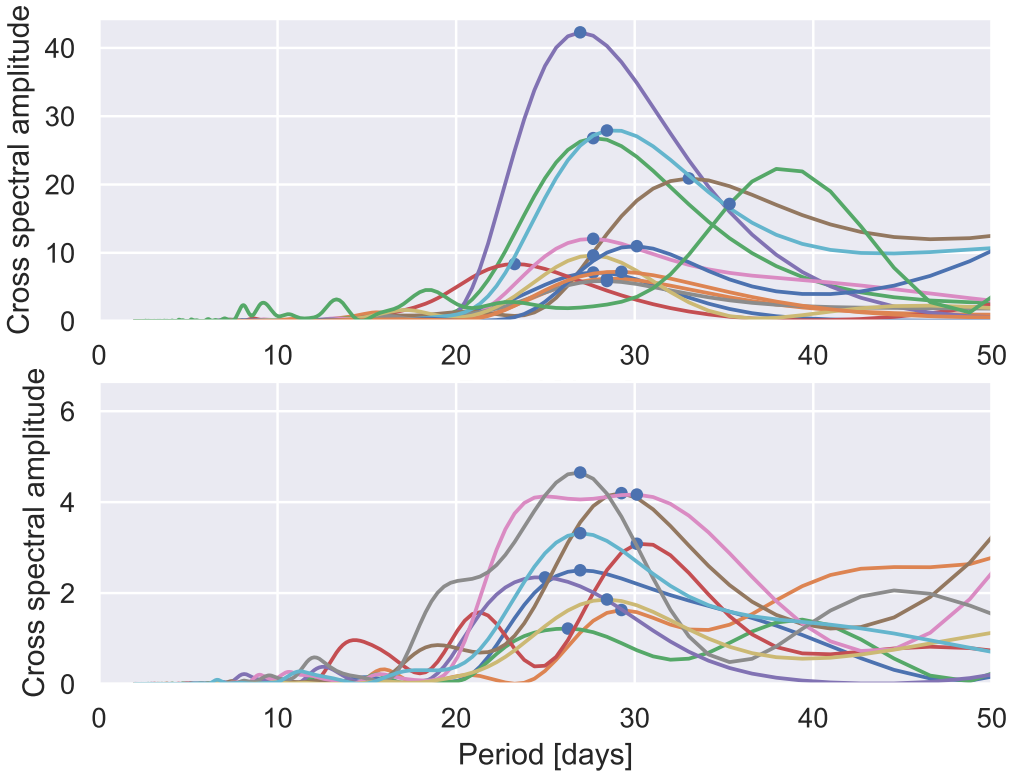

Figure 17: Cross-spectra of the 60-day lagged correlation between the meridional mean wind and $Y_{10.7}$ from 1994 through 2016. The period with the highest amplitude between 23 and 36 days is marked with a blue point.

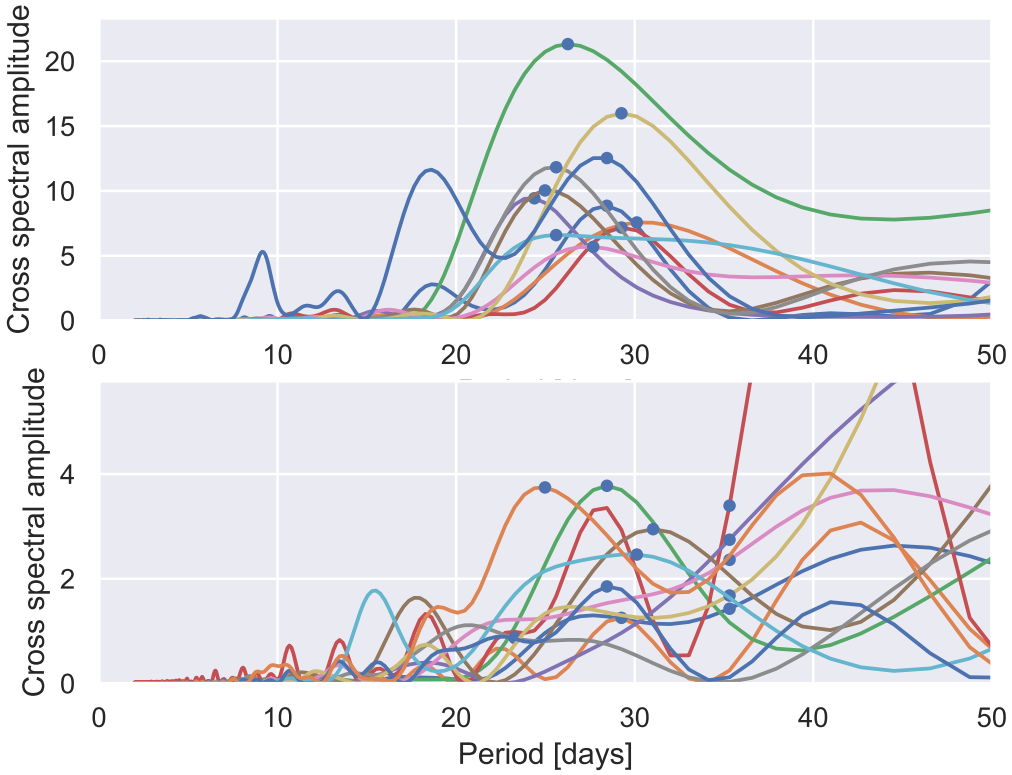

Figure 18: Cross-spectra of the 60-day lagged correlation between the zonal mean wind and $Y_{10.7}$ from 1994 through 2016. The period with the highest amplitude between 23 and 36 days is marked with a blue point.

Figures 19 is the cross spectrum of the lagged cross-correlation with meridional cross-spectral amplitudes in figure 10.

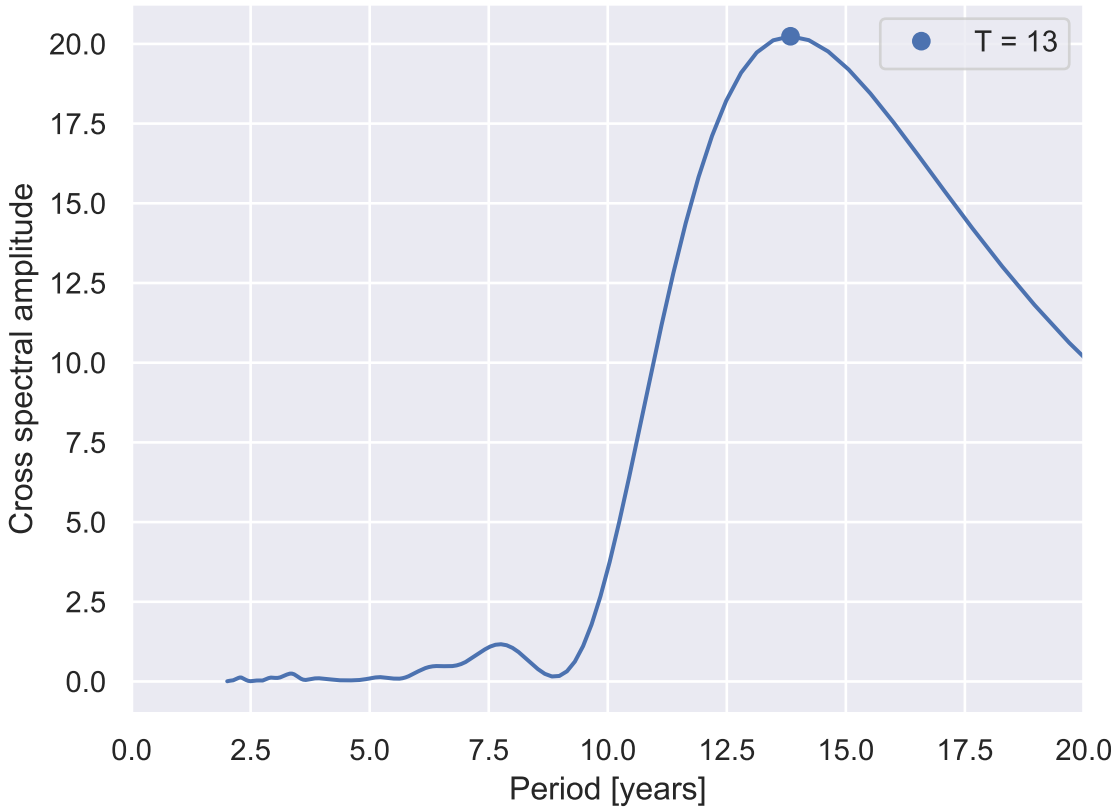

Figure 19: Power spectrum of the lagged correlation between the yearly maximal meridional power spectral amplitudes from figure 10 and $Y_{10.7}$. The period with the highest amplitude is marked with a blue point.

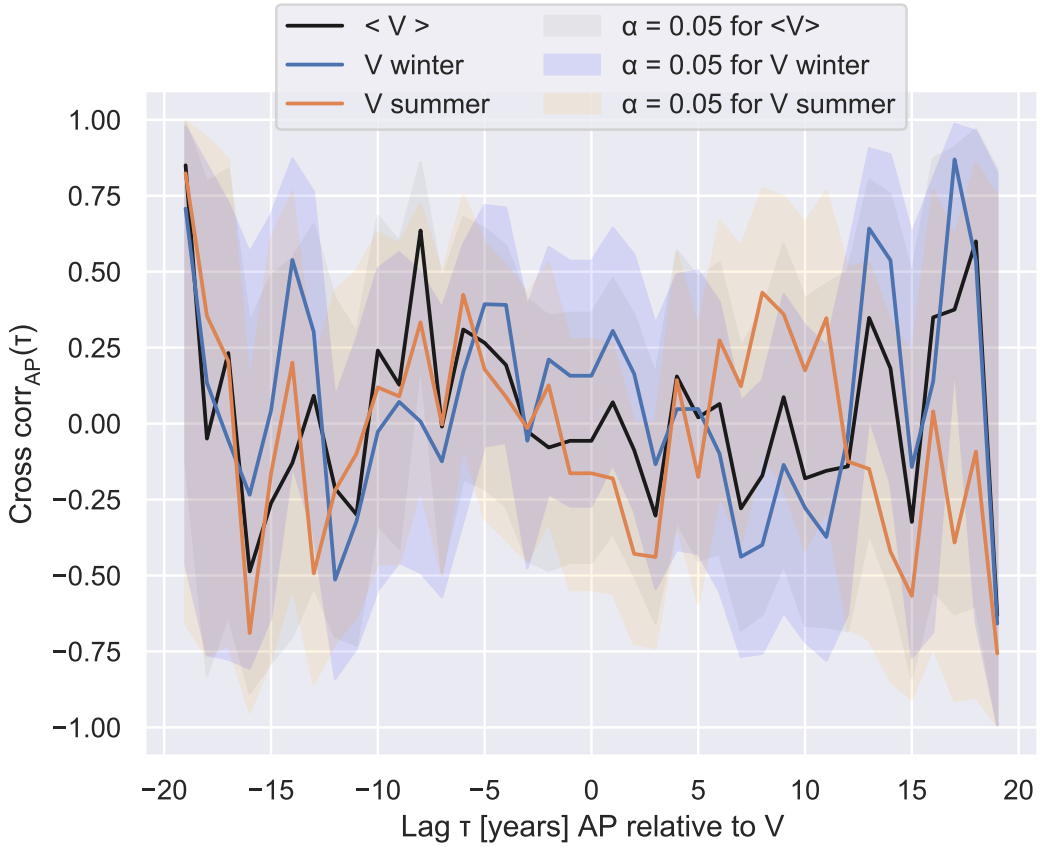

Figure 20: Cross-correlation with 95% confidence interval between yearly averages of AP and meridional wind averaged over full years, summer meridional wind and winter meridional wind. Negative lags refer to years AP leads the wind.

Figure 20 depicts the lagged cross-correlation between yearly averages; full year, winter and summer, of the meridional wind and $Y_{10.7}$, while figure 22 is the same for zonal wind. The cross-spectra of figure 20 are presented in 21 and for figure 22 in figure 23.

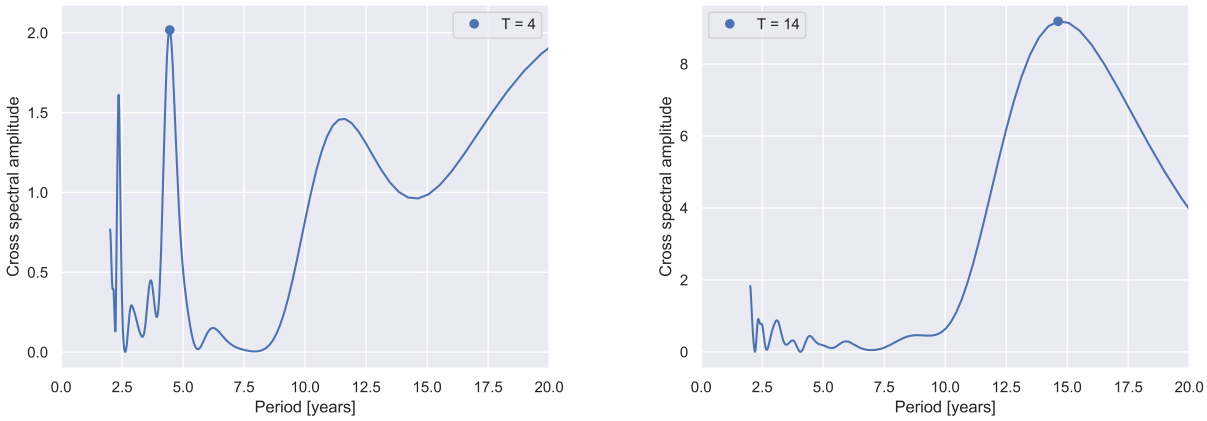

(a)

(b)

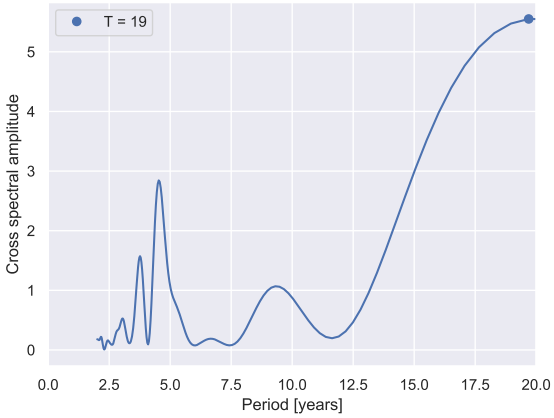

(c)

Figure 21: Cross spectral amplitude for the cross-correlation between yearly averages of AP and (a) mean meridional wind, (b) summer meridional wind and (c) winter meridional wind. The local maxima near eleven years are marked with blue points.

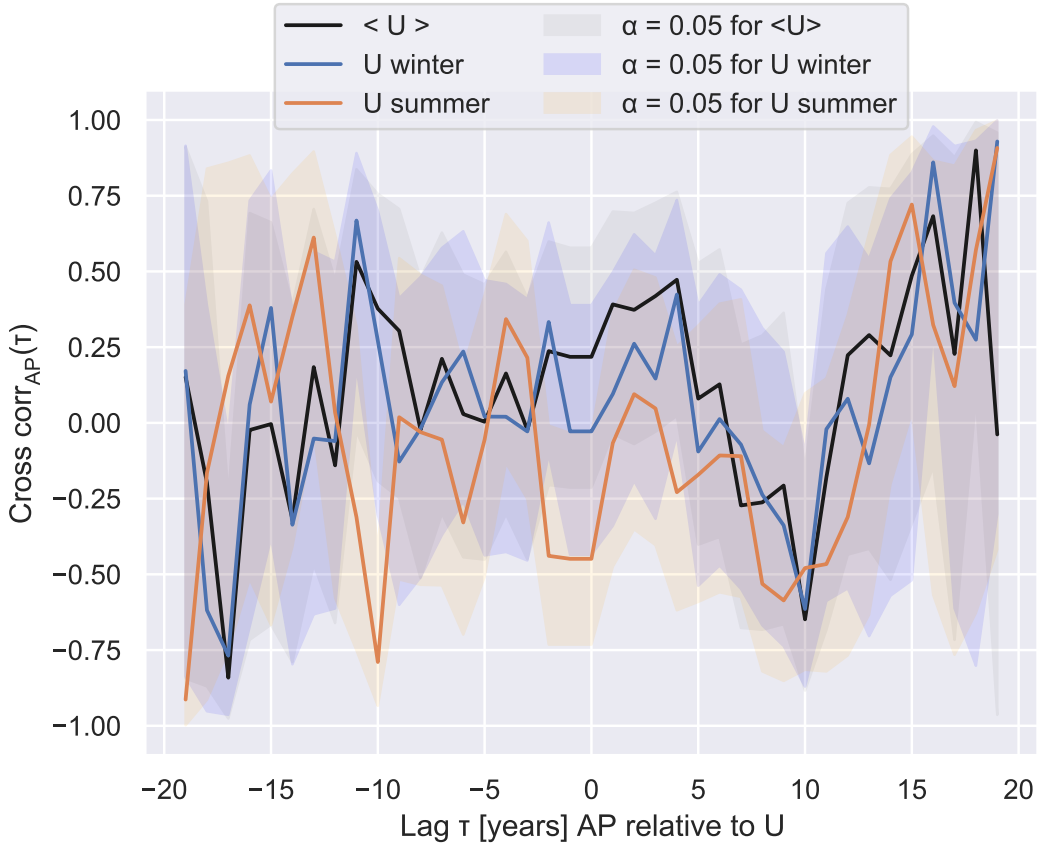

Figure 22: Cross-correlation with 95% confidence interval between yearly averages of AP and zonal wind averaged over full years, summer zonal wind and winter zonal wind. Negative lags refer to years AP leads the wind.

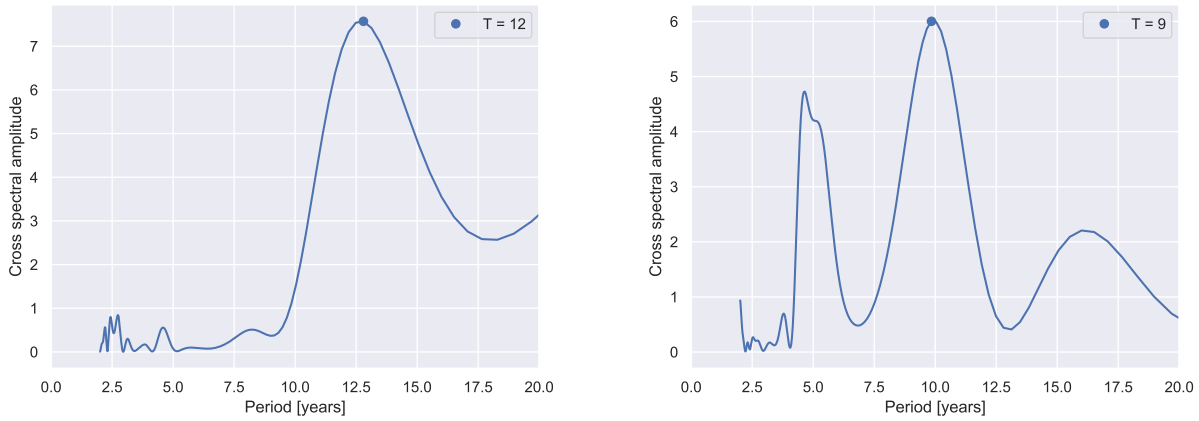

(a)

(b)

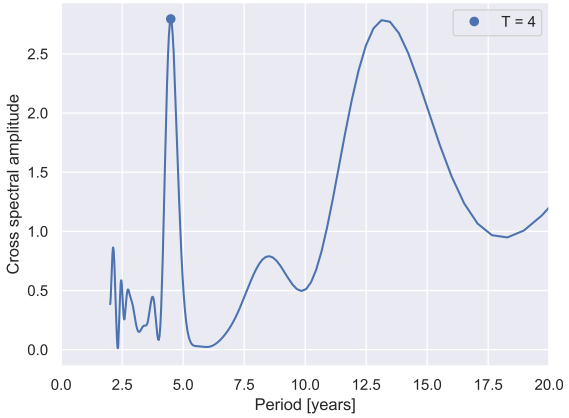

(c)

Figure 23: Cross spectral amplitude for the cross-correlation between yearly averages of AP and (a) mean zonal wind, (b) summer zonal wind and (c) winter zonal wind. The local maxima near eleven years are marked with blue points.

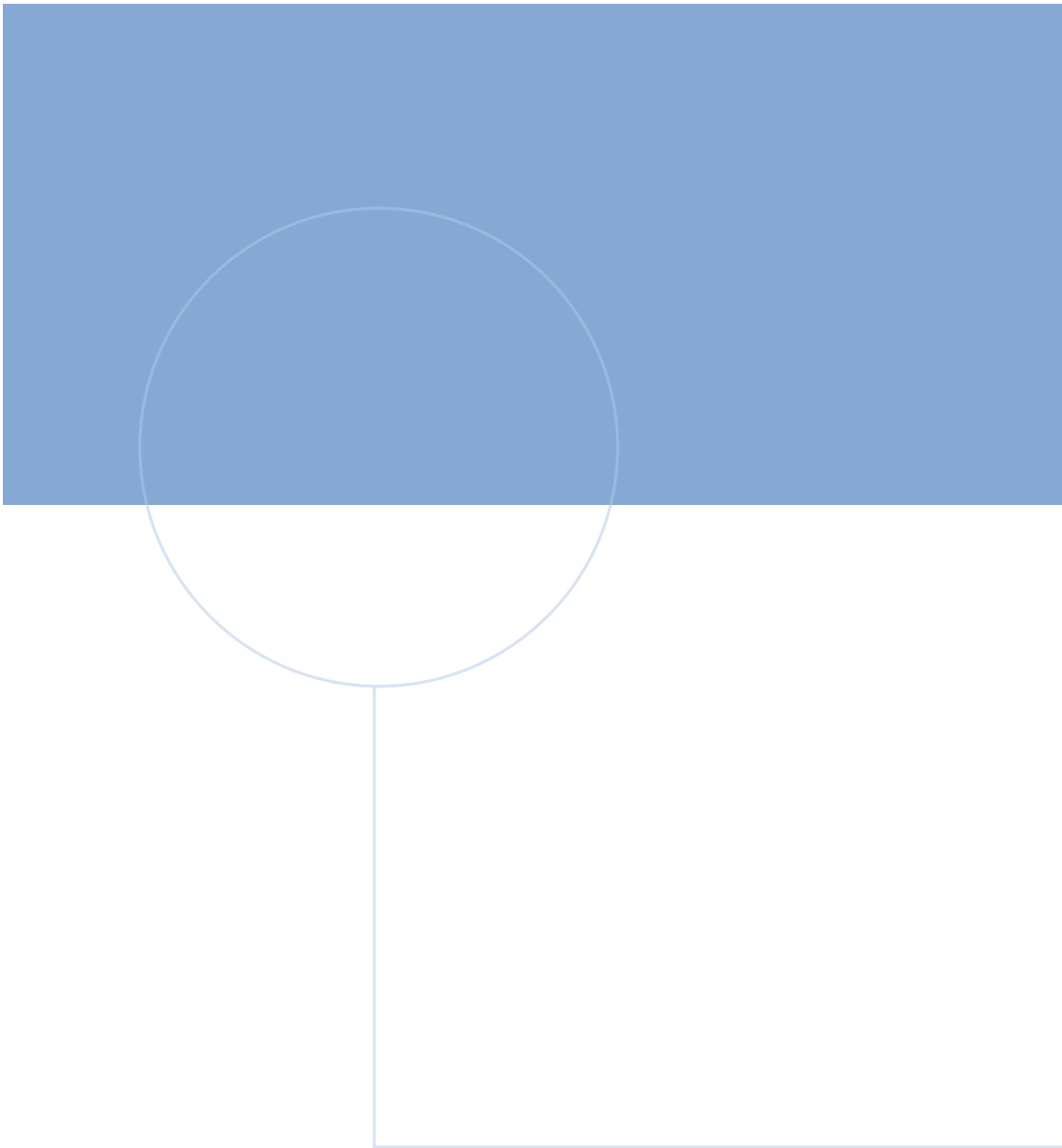

NTNU

Norwegian University of
Science and Technology